squares in the line that they intended to step on. Avoidance failure, therefore, resulted mainly from incorrect planning of the walking path from target to target and not from the wrong selection of a target from the three squares in a line due to age-related decline in visual acuity and/or visual search. Correlation analyses between each of the three measurements and standard clinical tests showed that the stepping and avoidance failures were correlated only mildly with several tests (Table 3). This was in contrast with the findings that the MTST performance time was highly correlated with all clinical tests. It seems that a decline in stepping accuracy results in an increased fall risk somewhat independently of the balance and gait features assessed by other standard clinical tests.

One possible explanation for the reason that measuring the stepping accuracy, particularly the stepping failure, could predict falls in spite of the multifocal etiology of falls was that these measurements could be associated directly with increased gait variability (1–3) and a decline in the visuomotor control of foot movement (4–6) in HR elderly individuals. This explanation was plausible, given that some clinical tests that have components of measuring the gait variability and visuomotor control of foot movement, such as the Dynamic Gait Index (28) or the Four Square Step Test (29), contributed to identifying HR elderly individuals.

In addition, some factors characterizing the MTST could make a significant contribution to enhance its predictive power. As in the W-TMT (12), to perform the MTST, the participants visually scanned the target while simultaneously attempting to step on it; participants would thus perform the MTST with the involvement of their executive functions. Due to an apparent decline in executive functions (12–15), HR elderly individuals would have difficulty walking in the MTST. Furthermore, the placement of multiple targets on a walkway could test the ability to step quickly in different directions. Because of the difficulty in maintaining a stabilized upright posture after stepping in different directions (29,30), especially with turning behavior (31), the HR elderly individuals may have less accurate stepping performance. To evaluate the validity of these possible explanations, future studies should investigate age-related changes in gaze behavior while performing the MTST; the frequency of turning behavior; and the functional relationship among the gaze, turning behavior, and accuracy of stepping performance.

We failed to demonstrate an association between the number of retrospective falls and the number of stepping and avoidance failures; the HR single fallers showed significantly higher frequency of both types of failure. This was in contrast to the relatively small individual differences in other standard tests (Table 1). We have no clear explanation for the reasons for such large individual differences; future studies should address this issue to reliably predict future falls on the basis of stepping and avoiding failures. Future studies should also address the possibility that the numbers of stepping and avoidance failures are associated with the circumstances under which falls occurred but not with the frequency of falls.

There are several issues that limit the conclusions to be drawn from this study. First, we measured only a single performance of the MTST from each participant; an examination of the within-participant reliability with a different walking path would be necessary in future research. Second, we did not measure participants' executive functions. Whether the difference in executive functions really underlies group differences between HR and LR elderly individuals should be a topic for future research.

In conclusion, the present findings provide general evidence that measuring the accuracy of foot placement while performing the MTST is potentially an effective clinical tool to identify HR elderly individuals. Possible explanations for the reason that measuring the stepping accuracy, especially the stepping failure, could predict falls would be (a) these measurements could be associated directly with increased gait variability and a decline in visuomotor control of foot movement in HR elderly individuals and (b) performing the MTST required the involvement of executive functions to find a footfall target. However, several findings, such as the lack of an association between the number of retrospective falls and the number of stepping and avoidance failures or the very large range in 95% CI observed in the logistic regression analysis, also suggest that the present results need to be interpreted cautiously.

References

1. Hausdorff JM, Rios DA, Edelberg HK. Gait variability and fall risk in community-living older adults: a 1-year prospective study. *Arch Phys Med Rehabil*. 2001;82(8):1050–1056.
2. Verghese J, Holtzer R, Lipton RB, Wang C. Quantitative gait markers and incident fall risk in older adults. *J Gerontol A Biol Sci Med Sci*. 2009;64(8):896–901.
3. Brach JS, Perera S, Studenski S, et al. Meaningful change in measures of gait variability in older adults. *Gait Posture*. 2010;31(2):175–179.
4. Chapman GJ, Hollands MA. Evidence for a link between changes to gaze behaviour and risk of falling in older adults during adaptive locomotion. *Gait Posture*. 2006;24(3):288–294.
5. Chapman GJ, Hollands MA. Evidence that older adult fallers prioritise the planning of future stepping actions over the accurate execution of ongoing steps during complex locomotor tasks. *Gait Posture*. 2007;26(1):59–67.
6. Chapman GJ, Hollands MA. Age-related differences in stepping performance during step cycle-related removal of vision. *Exp Brain Res*. 2006;174(4):613–621.
7. Marigold DS, Patla AE. Age-related changes in gait for multi-surface terrain. *Gait Posture*. 2008;27(4):689–696.
8. Di Fabio RP, Greany JF, Zampieri C. Saccade-stepping interactions revise the motor plan for obstacle avoidance. *J Mot Behav*. 2003;35(4):383–397.
9. Galna B, Peters A, Murphy AT, Morris ME. Obstacle crossing deficits in older adults: a systematic review. *Gait Posture*. 2009;30(3):270–275.
10. Kelly VE, Schrager MA, Price R, Ferrucci L, Shumway-Cook A. Age-associated effects of a concurrent cognitive task on gait speed and stability during narrow-base walking. *J Gerontol A Biol Sci Med Sci*. 2008;63(12):1329–1334.
11. Menant JC, St George RJ, Fitzpatrick RC, Lord SR. Impaired depth perception and restricted pitch head movement increase obstacle

contacts when dual-tasking in older people. *J Gerontol A Biol Sci Med Sci*. 2010;65(7):751–757.
12. Alexander NB, Ashton-Miller JA, Giordani B, Guire K, Schultz AB. Age differences in timed accurate stepping with increasing cognitive and visual demand: a walking trail making test. *J Gerontol A Biol Sci Med Sci*. 2005;60(12):1558–1562.
13. Persad CC, Giordani B, Chen HC, et al. Neuropsychological predictors of complex obstacle avoidance in healthy older adults. *J Gerontol B Psychol Sci Soc Sci*. 1995;50(5):P272–P277.
14. Persad CC, Jones JL, Ashton-Miller JA, Alexander NB, Giordani B. Executive function and gait in older adults with cognitive impairment. *J Gerontol A Biol Sci Med Sci*. 2008;63(12):1350–1355.
15. Persad CC, Cook S, Giordani B. Assessing falls in the elderly: should we use simple screening tests or a comprehensive fall risk evaluation? *Eur J Phys Rehabil Med*. 2010;46(3):457–460.
16. Herman T, Mirelman A, Giladi N, Schweiger A, Hausdorff JM. Executive control deficits as a prodrome to falls in healthy older adults: a prospective study linking thinking, walking, and falling. *J Gerontol A Biol Sci Med Sci*. 2010;65(10):1086–1092.
17. van Iersel MB, Kessels RP, Bloem BR, Verbeek AL, Olde Rikkert MG. Executive functions are associated with gait and balance in community-living elderly people. *J Gerontol A Biol Sci Med Sci*. 2008; 63(12):1344–1349.
18. Hajjar I, Yang F, Sorond F, et al. A novel aging phenotype of slow gait, impaired executive function, and depressive symptoms: relationship to blood pressure and other cardiovascular risks. *J Gerontol A Biol Sci Med Sci*. 2009;64(9):994–1001.
19. Li KZ, Roudaia E, Lussier M, et al. Benefits of cognitive dual-task training on balance performance in healthy older adults. *J Gerontol A Biol Sci Med Sci*. 2010;65(12):1344–1352.
20. Podsiadlo D, Richardson S. The timed "up & go": a test of basic functional mobility for frail elderly persons. *J Am Geriatr Soc*. 1991;39(2): 142–148.
21. Duncan PW, Studenski S, Chandler J, Prescott B. Functional reach: predictive validity in a sample of elderly male veterans. *J Gerontol*. 1992;47(3):M93–M98.
22. Vellas BJ, Wayne SJ, Romero L, et al. One-leg balance is an important predictor of injurious falls in older persons. *J Am Geriatr Soc*. 1997;45(6):735–738.
23. Lopopolo RB, Greco M, Sullivan D, Craik RL, Mangione KK. Effect of therapeutic exercise on gait speed in community-dwelling elderly people: a meta-analysis. *Phys Ther*. 2006;86(4):520–540.
24. Kalbe E, Calabrese P, Scgwalen S, Kessler J. The rapid dementia screening test (RDST): a new economical tool for detecting possible patients with dementia. *Dement Geriatri Cogn Disord*. 2003;16:193–199.
25. Shumway-Cook A, Brauer S, Woollacott M. Predicting the probability for falls in community-dwelling older adults using the timed up & go test. *Phys Ther*. 2000;80(9):896–903.
26. Guideline for the prevention of falls in older persons. American Geriatrics Society, British Geriatrics Society, and American Academy of Orthopaedic Surgeons Panel on Falls Prevention. *J Am Geriatr Soc*. 2001;49:664–672.
27. Naessens JM, O'Byrne TJ, Johnson MG, et al. Measuring hospital adverse events: assessing inter-rater reliability and trigger performance of the Global Trigger Tool. *Int J Qual Health Care*. 2010;22(4):266–274.
28. Shumway-Cook A, Woollacott M. *Motor Control: Theory and Practical Applications*; Baltimore, MD: Williams & Wilkins; 1995.
29. Dite W, Temple VA. A clinical test of stepping and change of direction to identify multiple falling older adults. *Arch Phys Med Rehabil*. 2002;83(11):1566–1571.
30. Tseng SC, Stanhope SJ, Morton SM. Impaired reactive stepping adjustments in older adults. *J Gerontol A Biol Sci Med Sci*. 2009;64(7): 807–815.
31. Taylor MJ, Dabnichki P, Strike SC. A three-dimensional biomechanical comparison between turning strategies during the stance phase of walking. *Hum Mov Sci*. 2005;24(4):558–573.

Oncogene (2011) 30, 4015–4025

www.nature.com/onc

ORIGINAL ARTICLE

Identification of AFAP1L1 as a prognostic marker for spindle cell sarcomas

M Furu[1,2,11], Y Kajita[1,3,11], S Nagayama[4], T Ishibe[1,2], Y Shima[1,2], K Nishijo[1,2], D Uejima[1,5], R Takahashi[1,4], T Aoyama[1,5], T Nakayama[2], T Nakamura[2], Y Nakashima[6], M Ikegawa[7], S Imoto[8], T Katagiri[9,12], Y Nakamura[9] and J Toguchida[1,2,10]

[1]Department of Tissue Regeneration, Institute for Frontier Medical Sciences, Kyoto University, Kyoto, Japan; [2]Department of Orthopaedic Surgery, Graduate School of Medicine, Kyoto University, Kyoto, Japan; [3]Department of Urology, Graduate School of Medicine, Kyoto University, Kyoto, Japan; [4]Department of Surgery, Graduate School of Medicine, Kyoto University, Kyoto, Japan; [5]Department of Orthopaedic Surgery, Kansai Medical University, Osaka, Japan; [6]Department of Diagnostic Pathology, Kyoto University Hospital, Kyoto, Japan; [7]Department of Genomic Medical Sciences, Graduate School of Medical Science, Kyoto Prefectural University of Medicine, Kyoto, Japan; [8]Laboratory for DNA Information Analysis, Human Genome Center, Institute of Medical Science, The University of Tokyo, Kyoto, Japan; [9]Laboratory of Molecular Medicine, Human Genome Center, Institute of Medical Science, The University of Tokyo, Kyoto, Japan and [10]Center for iPS Cell Research and Application, Kyoto University, Kyoto, Japan

Spindle cell sarcomas consist of tumors with different biological features, of which distant metastasis is the most ominous sign for a poor prognosis. However, metastasis is difficult to predict on the basis of current histopathological analyses. We have identified actin filament-associated protein 1-like 1 (AFAP1L1) as a candidate for a metastasis-predicting marker from the gene expression profiles of 65 spindle cell sarcomas. A multivariate analysis determined that AFAP1L1 was an independent factor for predicting the occurrence of distant metastasis ($P = 0.0001$), which was further confirmed in another set of 41 tumors by a quantitative mRNA expression analysis. Immunohistochemical staining using paraffin-embedded tumor tissues revealed that the metastasis-free rate was significantly better in tumors negative for AFAP1L1 ($P = 0.0093$ by log-rank test). Knocking down the *AFAP1L1* gene in sarcoma cells resulted in inhibition of the cell invasion, and forced expression of AFAP1L1 in immortalized human mesenchymal stem cells induced anchorage-independent growth and increased cell invasiveness with high activity levels of matrix metallopeptidase. Furthermore, tumor growth *in vivo* was accelerated in AFAP1L1-transduced sarcoma cell lines. These results suggest that AFAP1L1 has a role in the progression of spindle cell sarcomas and is a prognostic biomarker.

Oncogene (2011) **30,** 4015–4025; doi:10.1038/onc.2011.108; published online 25 April 2011

Keywords: AFAP1L1; spindle cell sarcoma; metastasis; prognostic marker

Correspondence: Professor J Toguchida, Institute for Frontier Medical Sciences, Kyoto University, 53 Kawahara-cho, Shogoin, Sakyo-ku, Kyoto 606-8507, Japan.
E-mail: togjun@frontier.kyoto-u.ac.jp
[11]These authors contributed equally to this work.
[12]Current address: Division of Genome Medicine, Institute for Genome Research, The University of Tokushima, Japan.
Received 27 October 2010; revised 11 February 2011; accepted 2 March 2011; published online 25 April 2011

Introduction

Sarcomas are non-epithelial malignant tumors that develop in mesenchymal tissue and classified into two groups on the basis of cellular morphology. Small round cell sarcomas, also known as blue tumors from their color on hematoxylin and eosin staining, include alveolar rhabdomyosarcomas and Ewing's sarcomas that develop in soft tissue and bone, respectively. Both have tumor-specific chromosomal translocations creating tumor-specific fusion genes (Helman and Meltzer, 2003; Toguchida and Nakayama, 2009). Spindle cell sarcomas, named for their flattened, elongated and fibroblastic morphology, far outnumber the first group. Malignant fibrous histiocytomas (MFHs) and ostesarcomas, the prototypes of this second group, develop in soft tissue and bone, respectively. They are generally radio- and chemoresistant, although high-dose, multidrug combination chemotherapy is effective for osteosarcomas. Except for some tumors, such as synovial sarcomas, which are characterized as having *SYT–SSX* fusion genes (Clark *et al.*, 1994), most spindle cell sarcomas lack tumor-specific genetic alterations (Toguchida and Nakayama, 2009). Mutations of tumor suppressor genes such as the *RB* and *p53* genes are found in many cases but not all (Toguchida *et al.*, 1992; Wadayama *et al.*, 1994). The histopathological complexity of soft tissue sarcomas is an issue. For example, MFH used to be considered the most prevalent soft tissue sarcoma but now the pathological concept is controversial (Fletcher *et al.*, 2001). To overcome this complexity, a number of gene expression profiling studies have been performed to classify spindle cell sarcomas and identify prognostic markers (Nielsen *et al.*, 2002; Lee *et al.*, 2004; Francis *et al.*, 2007; Nakayama *et al.*, 2007). Our group has also identified such markers using a custom-made cDNA microarray consisting of 23 040 genes in various types of malignant tumors (Nagayama *et al.*, 2002). As for synovial sarcomas, we have identified fibroblast growth factor (Ishibe *et al.*, 2005), Wnt-FZD10 (frizzled homolog 10) (Nagayama *et al.*, 2005) and retinoic acid

signals as molecular targets in synovial sarcomas (Ishibe *et al.*, 2008). For other types of tumors, however, the identification of tumor-specific markers is made difficult by small numbers of cases. Therefore, we have taken a different approach using the microarray data, trying to identify genes associated with aggressive phenotypes irrespective of the pathological diagnosis. Using distant metastasis as a discriminating factor, we have identified actin filament-associated protein 1-like 1 (AFAP1L1) as a candidate prognostic marker for spindle cell sarcomas. Here, we report that AFAP1L1 has a significant role in the progression of spindle cell sarcomas and is a prognostic marker as well as a potential target for molecular therapy.

Results

Identification of AFAP1L1 as a metastasis-related gene in spindle cell sarcomas

Genome-wide gene expression profiles of 65 soft tissue spindle cell sarcomas (STSs) were analyzed with a cDNA microarray system consisting of 23 040 genes, and mesenchymal stem cells (MSCs) were used as a reference (Nagayama *et al.*, 2002). The expression of each gene in tumor samples was demonstrated as the ratio of the signal intensity in tumor samples and MSCs (Nagayama *et al.*, 2002). Tumor samples were classified as positive for the gene if the ratio was more than 1.0, and negative if the ratio was 1.0 or less. Distant metastases developed in 29 cases, the remaining 36 patients being metastasis-free until the last follow-up (minimum of 61 months). The fraction of cases positive for each gene was calculated among tumors with and without metastasis, and statistical analyses were performed to identify genes associated with distant metastasis. This procedure identified the *AFAP1L1* gene, for which 21 of 29 cases with metastasis (Figure 1a) and 11 of 36 cases without metastasis (Figure 1b) were positive, and the difference was statistically significant ($P=0.0011$, Fisher's exact test). When the 65 cases were divided into AFAP1L1 (+) and AFAP1L1 (−) groups on the basis of the value relative to that of MSC, the metastasis-free fraction of AFAP1L1 (+) cases was lower than that of AFAP1L1 (−) cases (Figure 1c). AFAP1L1 is a member of the AFAP family along with AFAP-110 and AFAP1L2. AFAP-110 was identified as one of several major substrates of the viral oncogenic protein tyrosine kinase v-Src (Kanner *et al.*, 1990; Flynn *et al.*, 1993) and has been shown to function as an actin filament crosslinking protein with a fundamental role in the actin cytoskeleton's arrangement (Baisden *et al.*, 2001a). Moreover, it has been demonstrated that AFAP-110 is overexpressed in breast and prostate cancers and contributes to tumorigenic growth by regulating focal contact sites (Dorfleutner *et al.*, 2007; Zhang *et al.*, 2007). No previous reports concerning the function or involvement in cancer of AFAP1L1 have been published.

Although the overall amino-acid sequence similarity between AFAP-110 and AFAP1L1 is as much as 44%,

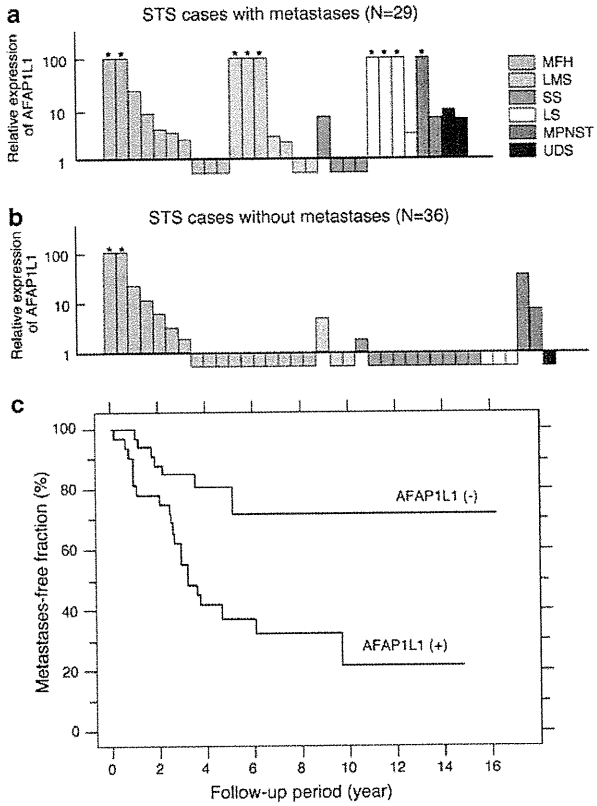

Figure 1 Identification of the *AFAP1L1* gene as a metastasis-associated gene of STSs. Expression of the *AFAP1L1* gene in STSs with metastasis ($N=29$) (**a**), and without metastasis ($N=36$) (**b**). The expression level of the *AFAP1L1* gene in each tumor is demonstrated relative to that in human bone marrow stem cells (hBMSCs). For convenience, the highest value is set as 100. Samples with a relative value of more than 100 are indicated by asterisks, and those with a relative value of less than 1.0, by rectangles. LMS, leiomyosarcoma; LS, liposarcoma; MFH, malignant fibrous histiocytoma; MPNST, malignant peripheral nerve sheath tumor; SS, synovial sarcoma; UDS, undifferentiated sarcoma. (**c**) Metastasis-free fraction of the initial set of STSs. A total of 65 STSs were divided by the expression level of the *AFAP1L1* gene relative to that in hBMSCs: the relative value in AFAP1L1 (+) tumors was more than 1.0 and the relative value in AFAP1L1 (−) tumors was equal to or less than 1.0. The metastasis-fee fraction of each group was demonstrated by a Kaplan–Meier curve.

AFAP1L1 shared most of the predicated domain structures with AFAP-110, such as two pleckstrin homology domains, two Src homology 2 domains (SH2), and a putative leucine zipper domain (Figure 2a) (Baisden *et al.*, 2001a). A polyclonal antibody was raised against its 79 N-terminal amino acids, which showed no homology with AFAP-110 (Figure 2a). Western blotting using this antibody showed a band with a molecular size of 90–100 kD in cell lines expressing the *AFAP1L1* gene (Figure 2b). When a set of sarcomas and human MSCs (hMSCs) were analyzed by quantitative PCR (qPCR), clear differences in the expression patterns between AFAP-110 and AFAP1L1 were found (Figure 2c). The expression of AFAP1L1 was much higher in sarcoma

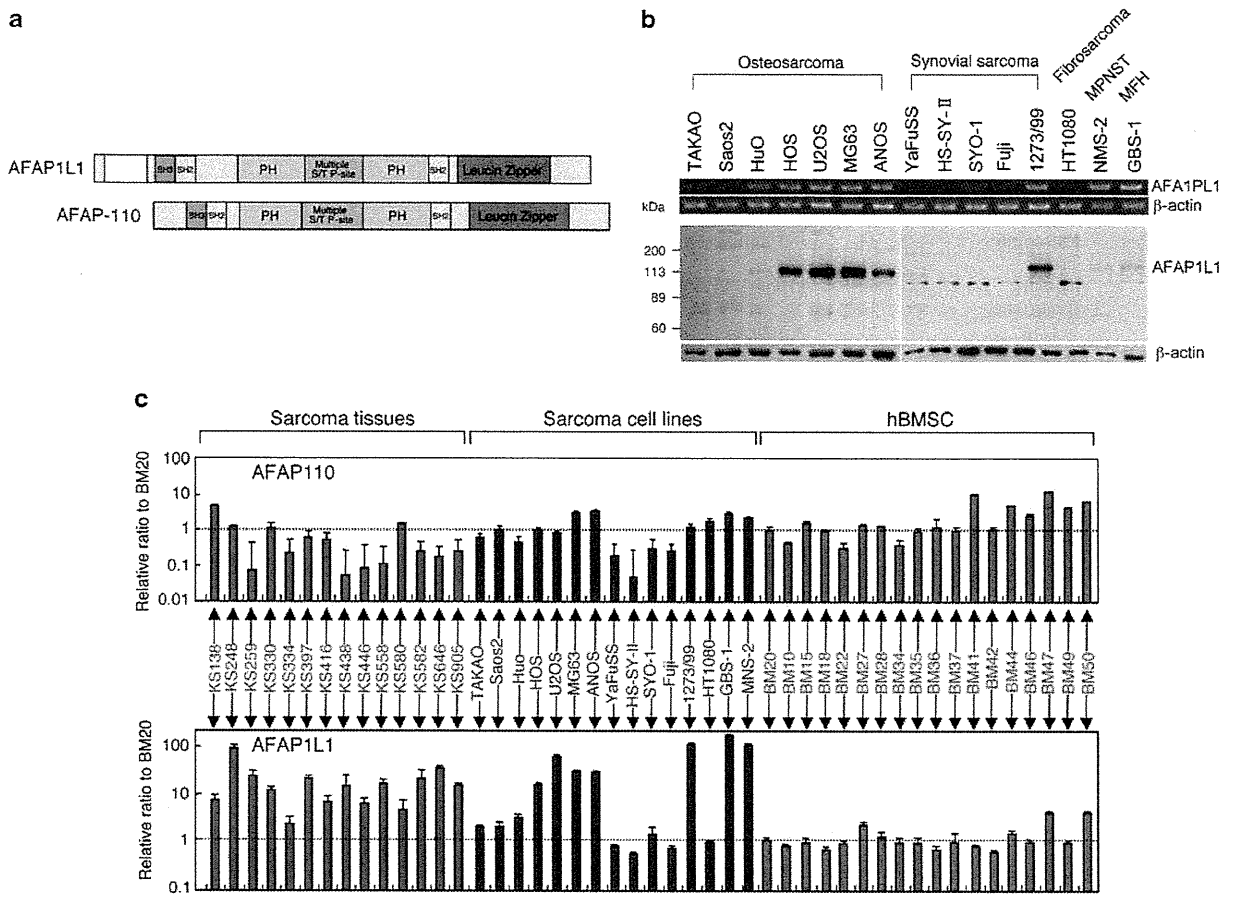

Figure 2 Comparison of AFAP-110 and AFAP1L1. (**a**) Predicted domain features of AFAP1L1 and AFAP-110. An oligopeptide derived from the hatched region was used as an antigen to raise a polyclonal antibody for APAP1L1.Validation of the anti-AFAP1L1 antibody. LZ, leucine zipper domain; PH, pleckstrin homology domain; SH2, Src homolog 2 motif. (**b**) Expression of AFAP1L1 in sarcoma cell lines. mRNA expression was analyzed by reverse transcription–PCR and protein expression was analyzed by western blotting using anti-AFAP1L1 antibody. β-Actin was used as a control. (**c**) Comparison of AFAP-110 and AFAP1L1 expression in cell lines and tissue samples. mRNA expression of AFAP-110 and AFAP1L1 in sarcoma tissues, sarcoma cell lines and human bone marrow stem cells (hBMSCs) was analyzed by qPCR. The expression level of each gene is demonstrated as a value relative to that in hBMSCs (BM20).

tissues and cell lines than in normal hMSCs ($P<0.0001$, Man–Whitney U test), whereas the expression of AFAP-110 was slightly higher in MSCs than in sarcoma tissues and cell lines ($P=0.0122$, Man–Whitney U test) (Figure 2c). On the basis of these results, we focused on the *AFAP1L1* gene.

Confirmation of the significance of AFAP1L1 in multivariate analyses

To confirm the significance of AFAP1L1 expression in the clinical behavior of STSs, the 65 cases were divided into two or more groups on the basis of clinicopathological factors, such as gender, age, location, size, depth, previous treatment history, surgery, and chemotherapy, pathological stage and pathological diagnosis, in addition to the expression of AFAP1L1 (Table 1). These factors were known to contribute to the prognoses in sarcoma patients (Ottaiano *et al.*, 2005). When the occurrence of distant metastases was used as an endpoint, AFAP1L1 expression was confirmed as a significant factor along with age and FNCLCC grade in univariate analyses (Table 1). These three factors were found to contribute independently to the prognosis in multivariate analyses (Table 1).

Association of AFAP1L1 expression with metastasis was confirmed in the second set of tumors

To confirm the significance of *AFAP1L1* gene expression, a second set of tumors consisting of 41 STSs was analyzed (Supplementary Table 1). Their clinical characteristics were almost equivalent to those of the tumors used in the initial analyses except for the pathological classification, due to a recent refinement of the diagnostic criteria for MFH (Fletcher *et al.*, 2002). STSs with no definitive features, which might be diagnosed as MFHs, were classified as 'undifferentiated sarcomas' in

Table 1 Cox's proportional hazards model analysis of factors relating to distant metastases in patients with STS

Variables	*Classes*	*No. of cases*	*Comparison*	*Hazard ratio*	*95% CI*	*Unfavorable/ Favorable*		P-*value*
Univariate analysis								
Gender	Female	39	Female vs male	0.872	0.416–1.828			0.7173
	Male	26						
Age	>60	31	≧60 vs <60	2.411	1.116–5.208	≧60	60>	0.0251
	<60	34						
Location	Extremities	44	Extremities vs trunk	0.759	0.350–1.645			0.4840
	Trunk	21						
History	Primary	49	Primary vs recurrence	1.212	0.517–2.843			0.6578
	Recurrence	16						
Size	>5 cm	51	≧5 cm vs <5 cm	1.787	0.620–5.154			0.2826
	<5 cm	14						
Depth	Superficial	24	Superficial vs deep	1.185	0.550–2.552			0.6640
	Deep	41						
FNCLCC	Grade 1	9	Grade 3 vs others	2.652	1.259–5.587	Grade 3	Grade 1 or 2	0.0103
	Grade 2	28						
	Grade 3	28						
Surgery	Wide	33	Wide vs others	0.954	0.460–1.981			0.9004
	Marginal	29						
	Intralesional	3						
Chemotherapy	Performed	29	Performed vs not performed	0.639	0.298–1.367			0.2482
	Not performed	36						
Diagnoses	MFH	27	MFH vs others	0.709	0.329–1.527			0.3795
	Synovial sarcoma	14						
	Leiomyosarcoma	10						
	Liposarcoma	7						
	MPNST	4						
	UDS	3						
AFAP1L1	Positive	32	Positive vs negative	3.611	1.592–8.195	Positive	Negative	0.0021
	Negative	33						
Multivariate analysis								
Age				2.908	1.069–7.907	≧60	60>	0.0365
FNCLCC				3.607	1.409–9.231	Stage 3	Stage 1 or 2	0.0075
AFAP1L1				4.001	1.656–9.665	Positive	Negative	0.0021

Abbreviations: AFAP1L1, actin filament-associated protein 1-like 1; CI, confidence interval; FNCLCC, Fédération Nationale des Centres de Lutte Contre le Cancer; MFH, malignant fibrous histiocytoma; MPNST, malignant peripheral nerve sheath tumor; STS, soft tissue spindle cell sarcoma; UDS, undifferetiated sarcoma.

most cases. During the follow-up period (4–210 months for all patients; 29–210 months for living patients), 18 developed distant metastases and 23 were free from metastasis until the last follow-up, and the qPCR analysis was used to evaluate the expression of the *AFAP1L1* gene in tumors of each group. In all, 48 of 65 samples in the first set of tumors were available for the qPCR analysis, which showed that the expression level of the *AFAP1L1* gene was significantly higher in tumors with metastasis ($N=29$) than without ($N=19$) ($P=0.0347$, Man–Whitney U test) (Figure 3a). A similar difference was found in the second set of tumors: The expression level of the *AFAP1L1* gene was significantly higher in tumors with metastasis ($N=23$) than without metastasis ($N=19$) ($P=0.0093$, Man–Whitney U test). Therefore, the association of *AFAP1L1* gene expression with metastatic activity was confirmed in the second set of STSs.

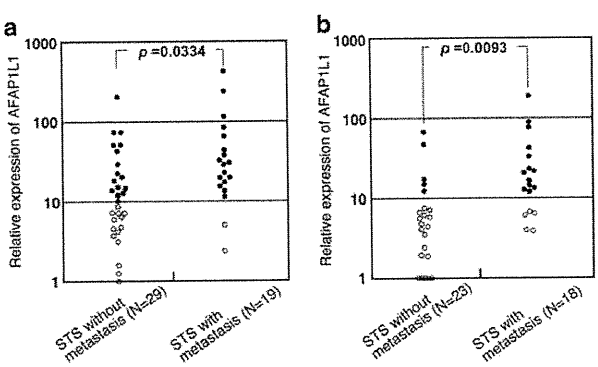

Figure 3 qPCR analyses of AFAP1L1 expression in STS. The expression level of the *AFAP1L1* gene in the first (**a**) and second (**b**) sets of STSs is demonstrated relative to that in human bone marrow stem cells.

Immunohistochemical analysis of AFAP1L1 protein in sarcomas

The expression of the AFAP1L1 protein was analyzed in paraffin-embedded specimens of 36 STSs from the second set of tumors, in which AFAP1L1 had already been analyzed by qPCR. On the basis of staining intensity of positive cells, tumors were classified into four groups; negative (−, 15 cases), weakly positive (+, 6 cases), moderately positive (++, 10 cases), and

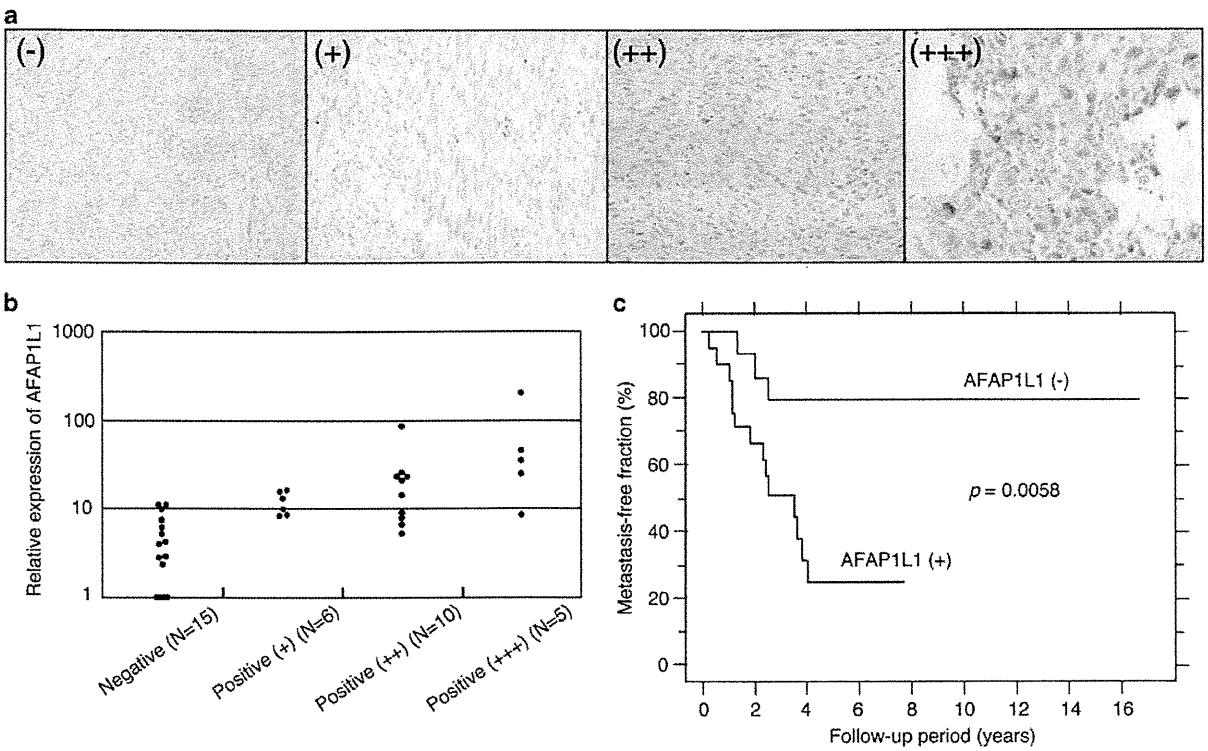

Figure 4 Expression of the AFAP1L1 protein in tumor tissues. (**a**) Expression of the AFAP1L1 protein in tumor tissues. Representative cases with negative (−), weak (+), moderate (+ +) or strong (+ + +) staining of AFAP1L1 are shown. (**b**) Relationship between the mRNA expression and immunostaining of AFAP1L1 in tumors. The mRNA level of the *AFAP1L1* gene in tumors used in the immunohistochemical analyses is demonstrated relative to that in human bone marrow stem cells. (**c**) Metastasis-free fraction of tumors with positive and negative staining of the AFAP1L1 protein. In all, 36 tumors were divided into AFAP1L1-negative (−; 15 cases) and -positive (+, + +, or + + +; 21 cases) groups, and the metastasis-fee fraction of each group was demonstrated by a Kaplan–Meier curve.

strongly positive (+ + +, 5 cases) (Figure 4a). The staining intensity of each tumor was consistent with the result of qPCR (Figure 4b). In positive cases, AFAP1L1 was detected predominantly in the cytoplasm of tumor cells. When tumors were simply divided into AFAP1L1-negative (−, 15 cases) and positive cases (+, + + and + + +, 21 cases), the stepwise regression model showed that the metastasis-free fraction of AFAP1L1-negative cases was significantly higher than that of positive cases (Figure 4c). There was no significant difference between tumors positive and negative for the staining in terms of patient's age, tumor size and tumor depth. As for FNCLCC grade, however, the number of high-grade tumor (grade 3) in positive cases (12/21 cases) was significantly higher than that in negative cases (3/15 cases) ($P = 0.0407$, Fisher's exact test). Therefore, the association of AFAP1L1 expression with metastasis was confirmed by both mRNA and protein analyses, suggesting AFAP1L1 to be a prognostic marker of spindle cell sarcomas.

Inhibition of AFAP1L1 expression reduced the invasiveness

We next generated AFAP1L1-knocked down cells to investigate the function of AFAP1L1 using an RNA interference system mediated by a lentivirus. U2OS and 1273/99 cells were used in these experiments because they had abundant AFAP1L1 expression among sarcoma cell lines tested (Figure 5a). Two non-targeting sequences for mammalian genes (control RNAi-1 and -2) and two AFAP1L1-targeting sequences (AFAP1L1 RNAi-1 and -2) were employed for further experiments. The transduction efficiency was 90–95% in U2OS cells and 85–90% in 1273/99 cells, as determined by counting EmGFP-positive cells (data not shown), and the knockdown of AFAP1L1 was confirmed effective by western blotting (Figure 5a). As for proliferative ability, no differences were found between the AFAP1L1-knockdown cells and control cells in the U2OS (Figure 5b) and 1273/99 cell lines (data not shown). However, matrigel invasion assays revealed that knocking down AFAP1L1 resulted in reduced cell invasiveness (Figure 5c).

Induction of AFAP1L1 gene expression conferred invasiveness

The cells of origin for sarcomas remain unclear but one possible candidate is the MSC (Matushansky *et al.*, 2007), so we chose immortalized human MSCs (ihMSCs) as a recipient for AFAP1L1 transduction. ihMSCs were established in our laboratory and shown to be fully transformed when the activated H-*ras* gene had been

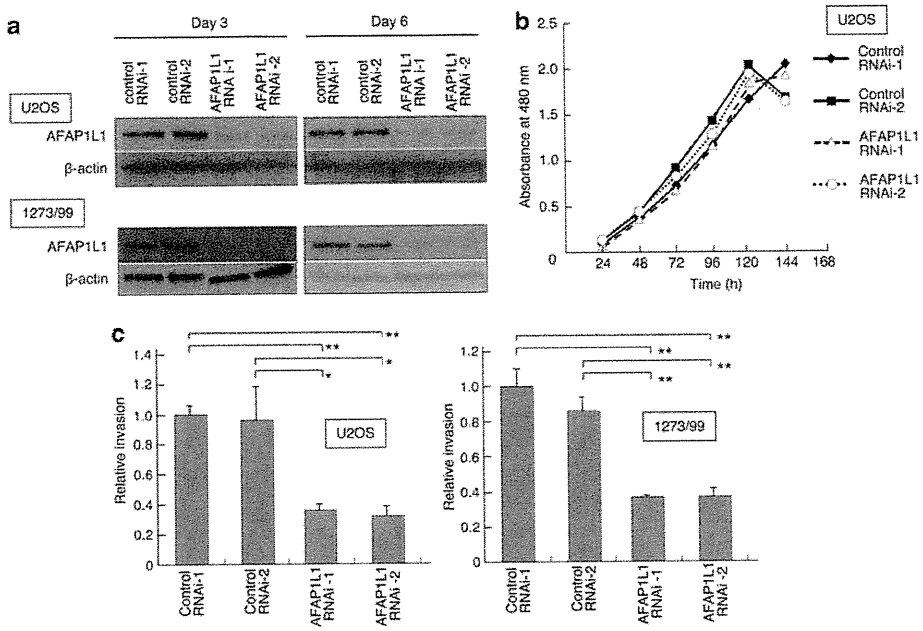

Figure 5 Downregulation of AFAP1L1 expression decreased invasiveness of sarcoma cells. (**a**) Western blotting of U2OS and 1273/99 cells transduced with microRNAs. Either non-targeting (control RNAi-1 or -2) or AFAP1L1-targeting (AFAP1L1 RNAi-1 or -2) microRNA was introduced and the expression of AFAP1L1 was analyzed 3 and 6 days later. (**b**) Growth curves of U2OS cells transduced with mircoRNAs. Cell viability was evaluated by WST-8 assay. (**c**) Invasive ability of U2OS and 1273/99 cells transduced with mircoRNAis. Matrix invasiveness was calculated as described in materials and methods, and demonstrated as fold change relative to control RNAi-1 cells. $^{**}P<0.01$; $^{*}P<0.05$.

introduced (Shima *et al.*, 2007). pLenti6/AFAP1L1 was transduced into ihMSCs, and several clones stably expressing AFAP1L1 were established (ihMSC/AFAP1L1) and used for further experiments (Figure 6a). The growth of AFAP1L1-transduced clones showed no significant change compared with that of the parental ihMSCs or ihMSC/LacZ cells (data not shown), whereas invasiveness and anchorage-independent growth were exaggerated in all four ihMSC/AFAP1L1 clones (Figures 6b and c).

Tumor invasiveness correlates with the activity of matrix metalloproteinases (MMPs), such as gelatinases, MMP-2 and MMP-9 (Egeblad and Werb, 2002; Overall and Kleifeld, 2006). To determine whether the increased invasive ability of the ihMSC/AFAP1L1 clones was related to increased excretion of MMPs, gelatin zymography was performed. The ihMSC/AFAP1L1 clones showed significantly increased activity of MMP-9 but not MMP-2 compared with control cells (Figure 6d). The increased excretion of MMP-9 in two ihMSC/AFAP1L1 clones was also confirmed by enzyme-linked immunosorbent assay (Figure 6e). These results suggest that AFAP1L1 endows ihMSCs with invasiveness, at least partly, by regulating MMP-9's excretion. In clinical samples, however, the expression level of MMP-9 was not clearly associated with that of AFAP1L1 ($R^2 = 0.248$) (Supplementary Figure S1).

Acceleration of tumor growth by AFAP1L1 expression in vivo

The inoculation of ihMSC/AFAP1L1 clones subcutaneously into immunodeficient mice produced no tumors (data not shown), indicating that the overexpression of AFAP1L1 in immortal cells was not enough for full transformation. To investigate whether AFAP1L1 modifies the phenotype of sarcoma cells without endogenous AFAP1L1 expression *in vivo*, stably expressing cell lines were generated using Saos2 cells as a recipient (Saos2/AFAP1L1) (Figure 7a). The growth of Saos2/AFAP1L1 clones *in vitro* showed no significant change compared with that of parental Saos2 or Saos2/LacZ control cells, but the invasive activity of Saos2/AFAP1L1 clones increased, which was consistent with that of ihMSC/AFAP1L1 clones (data not shown). These Saos2 clones were subcutaneously inoculated into the back of non-obese diabetic/severe combined immunodeficient mice to evaluate tumorigenesis and metastasis. Tumor growth was accelerated in Saos2/AFAP1L1 clones, although the extent of the increase seemed not to completely match the level of AFAP1L1 expression (Figures 7b and c). There was no metastasis by any Saos2/AFAP1L1 clones or control cells, suggesting that the expression of AFAP1L1 was not enough to produce distant metastasis in this animal model.

Discussion

Tumor type-specific molecular markers have been searched for in a variety of malignant tumors, in order to predict biological phenotype and/or serve as a target

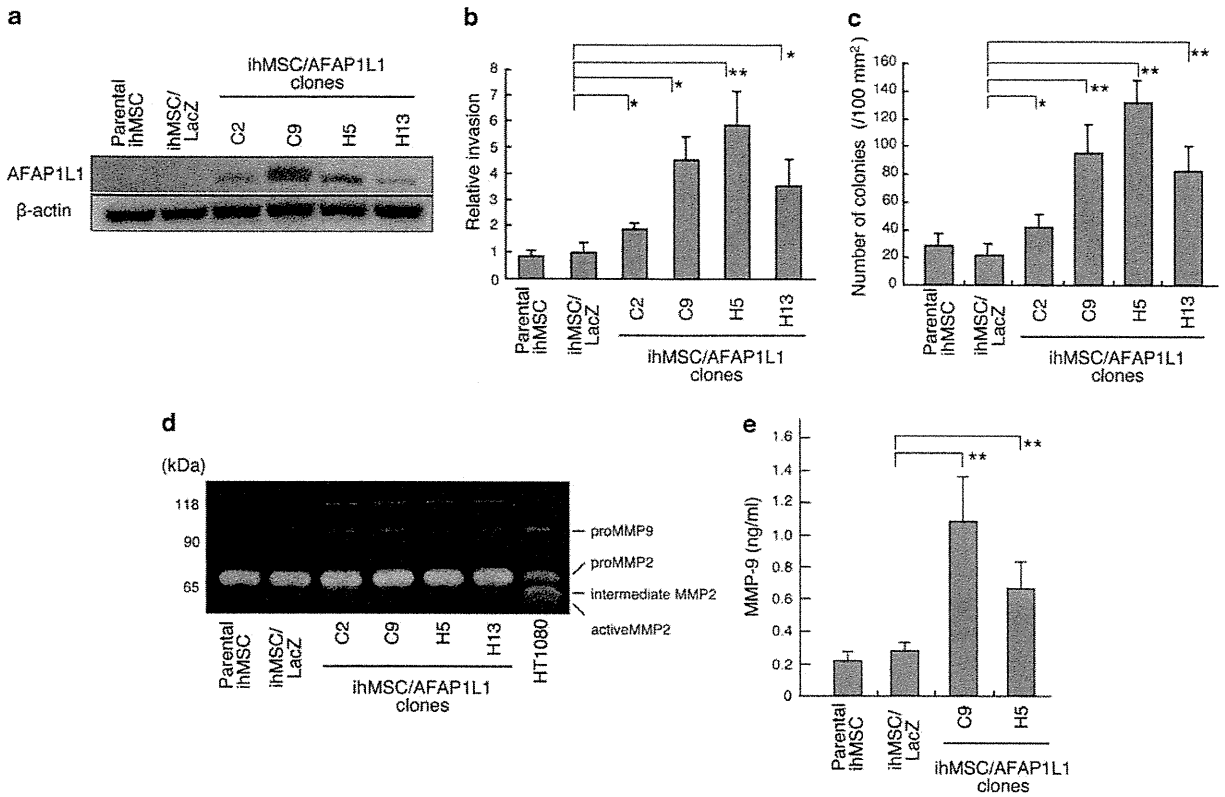

Figure 6 Upregulation of AFAP1L1 expression increased invasiveness and anchorage-independent growth of ihMSCs. (**a**) Western blotting of ihMSC clones stably expressing AFAP1L1. ihMSCs transduced with a LacZ-expressing lentivirus were used as a control. (**b**) Invasive ability of ihMSC clones transduced with AFAP1L1. Matrix invasiveness was calculated as described in materials and methods and demonstrated as fold change relative to LacZ-transduced cells. (**c**) Anchorage-independent growth of ihMSC clones transduced with AFAP1L1. (**d** and **e**) Production of MMP-9 in ihMSC clones transduced with AFAP1L1. Gelatin zymography (**d**) and enzyme-linked immunosorbent assay (**e**) demonstrated increased secretion of MMP-9 in ihMSC clones transduced with AFAP1L1. $^{**}P<0.01$; $^{*}P<0.05$.

for therapy. In the case of spindle cell sarcomas, however, the diversity and rarity of tumors have hampered such efforts. The importance of this study lies in having identified AFAP1L1 as a metastatic and a prognostic marker of spindle cell sarcomas, irrespective of pathological diagnosis. However, the significance of this gene in the development of distant metastasis should be carefully evaluated because our strategy focused on the contribution of single genes. Recently, two studies using large numbers of samples have been published relating to prognostic and therapeutic markers for soft tissue sarcomas. Barretina *et al.* (2010) performed an intensive analysis of 722 protein-coding and miRNA genes using a combination of DNA sequencing and a single-nucleotide polymorphism array and identified several tumor subtype-specific genetic alterations, some of which could be molecular targets for therapy. Chibon *et al.* (2010) identified a set of 67 genes on the basis of genomic and expression profiling and established a complexity index in sarcomas, which can predict the prognosis of patients. Among 67 genes, most were related to mitosis and chromosome management, and the *AFAP1L1* gene was not included.

Clinical results clearly demonstrated the association of AFAP1L1 with metastatic behavior of sarcomas in our cohorts, but the molecular mechanisms underlying this association are not yet clear. The results of knockdown and forced-expression experiments using sarcoma cell lines suggest that AFAP1L1 is involved in the process of invasion. Increased invasion of the matrix gel was confirmed in AFAP1L1-introduced ihMSC clones in association with an increase in excretion of MMP-9, a common feature of highly invasive malignant cells. We searched the ONCOMINE cancer array database (http://www.oncomine.org) and found a moderate correlation ($R^2 = 0.6964$) between AFAP1L1 and MMP-9 in glioblastomas (Sun *et al.*, 2006). We have no clear explanation of why we failed to find a clear association between the expression level of AFAP1L1 and that of MMP-9 in clinical samples (Supplementary Figure S1). This may be due to the multifactorial control of MMP-9 expression (St-Pierre *et al.*, 2004), and factors other than MMP-9 may be involved in the role of AFAP1L1 in tumor cell invasion. In this respect, it is intriguing that although the introduction of AFAP1L1 expression caused no change in growth profiles *in vitro*,

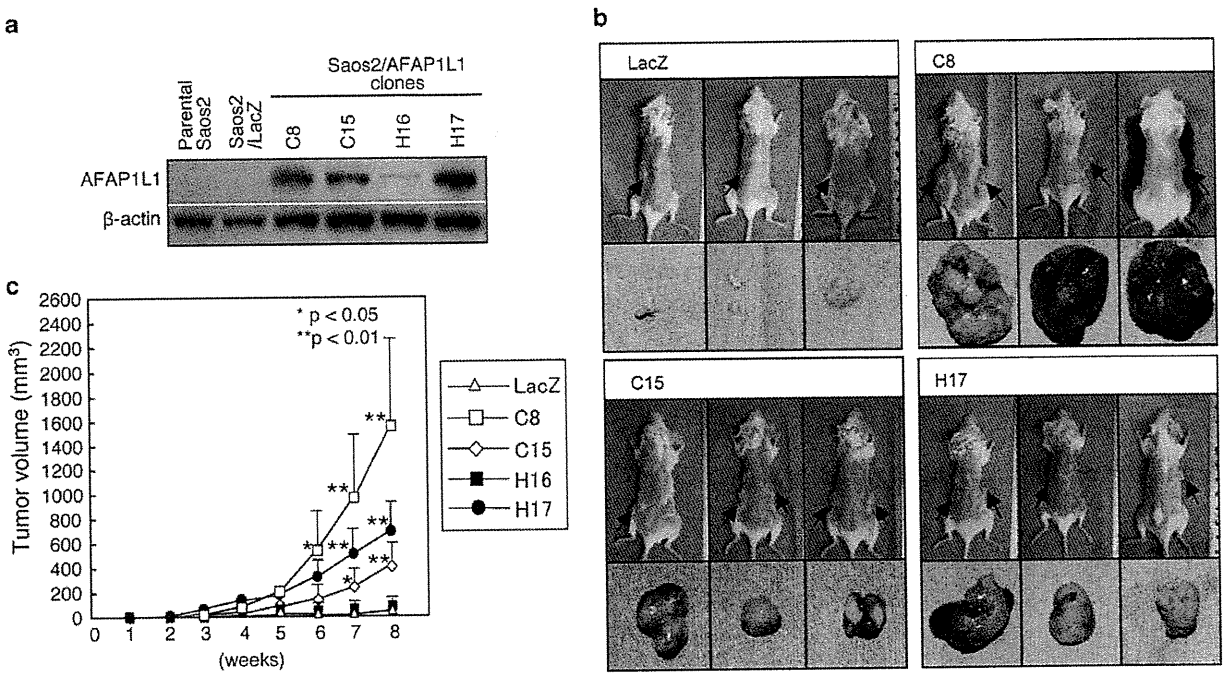

Figure 7 Acceleration of tumor growth by AFAP1L1 *in vivo*. (**a**) Western blotting of Saos2 clones stably expressing AFAP1L1. Saos2 cells transduced with a LacZ-expressing lentivirus were used as a control. (**b**) Macroscopic finding of tumors that developed in mice injected with AFAP1L1- or LacZ-transduced Saos2 clones. Tumors are indicated by arrows. (**c**) Growth curve of tumors shown in (**b**). $^{**}P<0.01$; $^{*}P<0.05$. Statistical examination was carried out by analysis of variance. Six mice were used for each cell clone.

the formation of tumor masses was accelerated *in vivo*. This suggested a role for AFAP1L1 at the interface between tumor cells and environments. Although the *AFAP1L1* gene was identified as a metastasis-associated gene from clinical data, we failed to find an association of metastasis with the expression of AFAP1L1 in experiments *in vivo*. The current experimental system using the subcutaneous inoculation of osteosarcomas cells may not be appropriate for evaluating the function of AFAP1L1.

AFAP1L1 is a paralogue of AFAP-110, which is an SH2/SH3-binding partner for Src (Flynn *et al.*, 1993; Guappone and Flynn, 1997; Qian *et al.*, 1998). AFAP-110 contains several protein-binding motifs at its amino terminus and functions as an adapter protein for actin filaments (Qian *et al.*, 2000; Baisden *et al.*, 2001b; Qian *et al.*, 2004). It is also required to control protein kinase Cα-mediated activation of c-Src and the subsequent formation of podosomes (Gatesman *et al.*, 2004). AFAP1L2, also known as XB130, is another paralogue of AFAP-110. AFAP1L2 associates with Src as well (Xu *et al.*, 2007) and is predominantly expressed in the thyroid (Lodyga *et al.*, 2009). AFAP1L2 cooperates with RET/PTC (rearranged in transformation/papillary thyroid carcinomas), a thyroid-specific tyrosine kinase, to increase phosphorylation of AKT, suggesting a role in thyroid cancer (Lodyga *et al.*, 2009). In addition, although AFAP1L2 has structural similarities to chicken AFAP-110 with which it was identified in a search of databases, it does not associate with actin filaments, suggesting a different role from that of AFAP-110 (Lodyga *et al.*, 2009). We have performed a series of experiments to examine the association of AFAP1L1 with actin filaments but found no definite evidence of one (data not shown). Although we speculate that AFAP1L1 acts as an adapter protein on the basis of its structural similarity to AFAP-110, AFAP1L1 functions in sarcoma cells via mechanisms distinct from those of AFAP-110, which may confer aggressive biological features.

Materials and methods

Clinical samples

Tumor samples were obtained at resection surgery in Kyoto University Hospital and preserved as described previously (Nagayama *et al.*, 2002). At least 90% of the viable cells in each specimen were identified as tumor cells. Primary hMSCs (hMSCs) were obtained and cultured by a method reported previously (Shibata *et al.*, 2007). All samples were approved for analysis by the ethics committee of the Faculty of Medicine, Kyoto University.

Cell lines

HS-SY-II was kindly provided by H Sonobe (Kochi University, Japan), SYO-1 by A Kawai (Okayama University, Japan), Fuji by S Tanaka (Hokkaido University, Japan), 1273/99 by O Larsson (Karolinska Institute, Sweden), NMS-2 (malignant peripheral nerve sheath tumor) by A Ogose (Niigata University, Japan) and GBS1 (MFH) by H Kanda (The Cancer Institute of the Japanese Foundation for Cancer

Research, Japan). ANOS, YaFuSS and an immortalized hMSC (ihMSC) line were established in our laboratory as described previously (Aoyama *et al*., 2004; Ishibe *et al*., 2005; Shima *et al*., 2007). Other cell lines were purchased from American Type Culture Collection (Manassas, VA, USA) or Japanese Collection of Research Bioresources (JCRB) (Ibaraki, Japan). Cells were maintained in RPMI 1640 medium or Dulbecco's modified Eagle's medium (DMEM, Sigma-Aldrich, St Louis, MO, USA) with 10% fetal bovine serum (HyClone, Thermo Fisher Scientific Inc., Waltham, MA, USA) at 37 °C under 5% CO_2.

Production of anti-AFAP1L1 polyclonal antibody
The polyclonal antibody for AFAP1L1 was raised by immunizing rabbits with glutathione *S*-transferase-fused polypeptides corresponding to codon 35–113 of the human *AFAP1L1* gene and purified with standard protocols using affinity columns.

Immunohistochemical and immunocytochemical analyses
Immunohistochemical experiments using paraffin-embedded specimens of soft tissue sarcomas were performed as described previously (Kohno *et al*., 2006). The anti-AFAP1L1 antibody was used at a concentration of 1 μg/ml. For immunocytochemistry, cells were fixed with 4% paraformaldehyde, permeabilized with 0.5% Triton X-100 and blocked with 1% bovine serum albumin in PBS. Slides were incubated with the anti-AFAP1L1 antibody or an anti-Flag M2 antibody (Sigma-Aldrich) overnight and then with a corresponding Alexa Fluor-conjugated secondary antibody (Invitrogen, Carlsbad, CA, USA). When indicated, rhodamine–phalloidin (Invitrogen) was used to stain actin fibers. Nuclei were stained with 4,6-diamidino-2-phenylindole. Cells were viewed with an IX81 (OLYMPUS, Tokyo, Japan) and photographed. The scoring was performed by two researchers without information on the clinical data for each sample.

Transient AFAP1L1 expression vectors
The coding region of the *AFAP1L1* gene was cloned into the pCAGGS vector (pCAG/AFAP1L1WT) tagged at the N-terminus with 3 × Flag. Transfection of these vectors was carried out using the Amaxa electroporation system (Amaxa Biosystems, Cologne, Germany) according to the manufacturer's instructions.

Lentiviral production
The BLOCK-iT Pol II miR RNAi Expression Vector Kit (Invitrogen) was used to knock down the *AFAP1L1* gene. Two oligonucleotides targeting AFAP1L1 (Hmi456004 and 456007, designated AFAP1L1 RNAi-1 and -2) and two control microRNAs that have no homology with mammalian gene sequences (designated control RNAi-1 and -2) were designed by and purchased from Invitrogen. They were annealed and ligated into the pcDNA6.2-GW/EmGFP-miR, in which microRNA expression was driven by a cytomegalovirus promoter with simultaneous expression of EmGFP. The cassette was subsequently cloned into pLenti6/V5-DEST, and cells were infected with supernatant containing microRNA lentiviruses (4.2×10^6 TU/ml) using the ViraPower Lentiviral Expression System (Invitrogen). These microRNA-transduced cells were prepared without drug selection or single-cell cloning. To generate cells stably expressing AFAP1L1, its gene was cloned into pLenti6/V5-DEST by a PCR-based method (pLenti6/AFAP1L1). As a control, a β-galactosidase gene-expressing vector (pLenti6/LacZ) was used. Cells were infected with these lentiviruses and selected with blasticidin (Invitrogen) for two weeks. Several clones of pLenti6/AFAP1L1-transduced cells were isolated by limiting dilution. pLenti6/LacZ-transduced control cells were used without cloning.

Western blot analyses
Western blot analyses were performed as described previously (Kohno *et al*., 2006). Membranes were incubated overnight with the anti-AFAP1L1 (1:1000), anti-Flag M2 (1:4000; Sigma-Aldrich) or anti-β-actin (1:4000; Sigma-Aldrich) antibody.

Matrigel invasion assay
Cell suspensions (2.5×10^4) in 0.5 ml of DMEM without fetal bovine serum were placed in the upper chambers of 8 μm control cell culture inserts (BD Biosciences, Franklin Lakes, NJ, USA) or BioCoat matrigel invasion chambers (BD Biosciences), and 0.5 ml of DMEM containing 5% fetal bovine serum was placed in each lower chamber. After incubation for 22 h at 37 °C under 5% CO_2, cells on the upper surface of the membrane were mechanically removed. The membranes were fixed, and stained with 1% Toluidine blue. Cells were counted in five randomly chosen fields under a magnification of × 100. Cell invasiveness was calculated by dividing the number of cells invading through the matrigel membrane by the number invading the control insert.

Cell growth assay
Cells were seeded on 96-well plates at a density of 1000 per well in quadriplicate. The next day, cell viability was assessed by WST-8 using a Cell Counting Kit (DOJINDO, Kumamoto, Japan) every 24 h, according to the manufacturer's instructions.

Colony formation in soft agar
Cells (1×10^4) were suspended in DMEM containing 0.35% agarose and layered on a solidified 0.7% agarose layer in 60-mm tissue culture plates and cultured at 37 °C under 5% CO_2. After 4 weeks of incubation, p-iodonitrotetrazolium violet (Sigma-Aldrich) was added to count viable colonies.

Gelatin zymography
Gelatinolytic activity of the supernatant was analyzed as described elsewhere. Briefly, cells (4×10^5) were incubated with DMEM containing 10% fetal bovine serum for 24 h and then the medium was replaced with 0.5 ml of OptiMEM1 (Invitrogen) containing 0.1% bovine serum albumin. After 16 h of incubation, the conditioned medium was analyzed on a 10% Tris–glycine gel containing 0.1% gelatin. The gel was treated with renaturating buffer for 30 min and with developing buffer for 12 h at 37 °C. Bands of gelatinolytic activity were visualized after staining the gels with 0.1% coomassie brilliant blue R-250 (Thermo Fisher Scientific Inc.) and then destaining. The digested bands were scanned by ChemiDocXRS (Bio-Rad Laboratories, Inc., Hercules, CA, USA).

Enzyme-linked immunosorbent assay
The expression of MMP-9 was quantified using a commercially available enzyme-linked immunosorbent assay system (Amersham matrix metalloproteinase-9 human biotrak ELISA system, GE Healthcare, Little Chalfont, UK) according to the manufacturer's instructions.

Animal experiments
All experiments with animals were approved by the Animal Research Committee (Graduate School of Medicine, Kyoto University) and conducted according to the Guidelines for Animal Experiments of Kyoto University. Cells (5×10^6)

suspended in 100 µl of PBS were injected subcutaneously into the hind flank region of female non-obese diabetic/Shi-*scid* Jic (non-obese diabetic/severe combined immunodeficient) mice at 5 weeks of age (Clea Japan, Tokyo, Japan). Tumor volumes were calculated using the formula: (length × width × height × 3.14)/6.

Reverse transcription and real-time qPCR

RNA extraction and reverse transcription were performed as described previously (Kohno *et al.*, 2006). Real-time qPCR analyses were performed with the ABI PRISM 7700 Sequence Detection System (Applied Biosystems, Carlsbad, CA, USA). Taqman probes for AFAP1L1 (5′-GGCCCTTCCTCTGGGA CCCGGC-3′) and AFAP-110 (Taqman Gene Expression Assays Hs00222181_m1) were purchased from Applied Biosystems. 18S rRNA was also purchased from Applied Biosystems and used as an endogenous reference. Information on primers is available upon request.

Statistical analyses

Statistical analyses were performed using StatView software (SAS Institute Inc., Cary, NC, USA). Univariate and multivariate analyses were performed using Cox's proportional hazards model. The statistical significance of Kaplan–Meier curves was assessed by log-rank (Mantel–Cox) test. For comparisons of two individual data points, a two-sided Student's *t*-test was applied to assess statistical significance. An analysis of variance with *post hoc* testing was used for comparisons of more than three.

Conflict of interest

The authors declare no conflict of interest.

Acknowledgements

We thank Drs H Sonobe, A Kawai, S Tanaka, O Larsson, A Ogose, and H Kanda for providing cell lines, and T Tsunoda and S Miyano for data analyses. This work was supported by Grants-in-aid for Scientific Research from the Ministry of Education, Culture, Sports, Science and Technology.

References

Aoyama T, Okamoto T, Nagayama S, Nishijo K, Ishibe T, Yasura K *et al.* (2004). Methylation in the core-promoter region of the chondromodulin-I gene determines the cell-specific expression by regulating the binding of transcriptional activator, Sp3. *J Biol Chem* **279**: 28789–28797.

Baisden JM, Gatesman AS, Cherezova L, Jiang BH, Flynn DC. (2001b). The intrinsic ability of AFAP-110 to alter actin filament integrity is linked with its ability to also activate cellular tyrosine kinases. *Oncogene* **20**: 6607–6616.

Baisden JM, Qian Y, Zot HM, Flynn DC. (2001a). The actin filament-associated protein AFAP-110 is an adaptor protein that modulates changes in actin filament integrity. *Oncogene* **20**: 6435–6447.

Barretina J, Taylor BS, Banerji S, Ramos AH, Lagos-Quintana M, DeCarolis PL *et al.* (2010). Subtype-specific genomic alterations define new targets for soft-tissue sarcoma therapy. *Nat Genet* **42**: 715–721.

Chibon F, Lagarde P, Salas S, Pérot G, Brouste V, Tirode F *et al.* (2010). Validated prediction of clinical outcome in sarcomas and multiple types of cancer on the basis of a gene expression signature related to genome complexity. *Nat Med* **16**: 781–787.

Clark J, Rocques PJ, Crew AJ, Gill S, Shipley J, Chan AM *et al.* (1994). Identification of novel genes, SYT and SSX, involved in the t(X;18)(p11.2;q11.2) translocation found in human synovial sarcoma. *Nat Genet* **7**: 502–508.

Dorfleutner A, Stehlik C, Zhang J, Gallick GE, Flynn DC. (2007). AFAP-110 is required for actin stress fiber formation and cell adhesion in MDA-MB-231 breast cancer cells. *J Cell Physiol* **213**: 740–749.

Egeblad M, Werb Z. (2002). New functions for the matrix metalloproteinases in cancer progression. *Nat Rev Cancer* **2**: 161–174.

Francis P, Namlos HM, Muller C, Eden P, Fernebro J, Berner JM *et al.* (2007). Diagnostic and prognostic gene expression signatures in 177 soft tissue sarcomas: hypoxia-induced transcription profile signifies metastatic potential. *BMC Genomics* **8**: 73.

Fletcher CD, Gustafson P, Rydholm A, Willen H, Akerman M. (2001). Clinicopathologic re-evaluation of 100 malignant fibrous histiocytomas: prognostic relevance of subclassification. *J Clin Oncol* **19**: 3045–3050.

Fletcher CDM, Unni KK, Mertens F. (2002). *Pathology and Genetics of Tumours of Soft Tissue and Bones.* IARC Press: Lyon.

Flynn DC, Leu TH, Reynolds AB, Parsons JT. (1993). Identification and sequence analysis of cDNAs encoding a 110-kilodalton actin filament-associated pp60src substrate. *Mol Cell Biol* **13**: 7892–7900.

Gatesman A, Walker VG, Baisden JM, Weed SA, Flynn DC. (2004). Protein kinase Calpha activates c-Src and induces podosome formation via AFAP-110. *Mol Cell Biol* **24**: 7578–7597.

Guappone AC, Flynn DC. (1997). The integrity of the SH3 binding motif of AFAP-110 is required to facilitate tyrosine phosphorylation by, and stable complex formation with, Src. *Mol Cell Biochem* **175**: 243–252.

Helman LJ, Meltzer P. (2003). Mechanisms of sarcoma development. *Nat Rev Cancer* **3**: 685–694.

Ishibe T, Nakayama T, Aoyama T, Nakamura T, Toguchida J. (2008). Neuronal differentiation of synovial sarcoma and its therapeutic application. *Clin Orthop Relat Res* **466**: 2147–2155.

Ishibe T, Nakayama T, Okamoto T, Aoyama T, Nishijo K, Shibata KR *et al.* (2005). Disruption of fibroblast growth factor signal pathway inhibits the growth of synovial sarcomas: potential application of signal inhibitors to molecular target therapy. *Clin Cancer Res* **11**: 2702–2712.

Kanner SB, Reynolds AB, Vines RR, Parsons JT. (1990). Monoclonal antibodies to individual tyrosine-phosphorylated protein substrated of oncogene-encoded tyrosine kinases. *Proc Natl Acad Sci USA* **87**: 3328–3332.

Kohno Y, Okamoto T, Ishibe T, Nagayama S, Shima Y, Nishijo K *et al.* (2006). Expression of claudin7 is tightly associated with epithelial structures in synovial sarcomas and regulated by an Ets family transcription factor, ELF3. *J Biol Chem* **281**: 38941–38950.

Lee YF, John M, Falconer A, Edwards S, Clark J, Flohr P *et al.* (2004). A gene expression signature associated with metastatic outcome in human leiomyosarcomas. *Cancer Res* **64**: 7201–7204.

Lodyga M, De Falco V, Bai XH, Kapus A, Melillo RM, Santoro M *et al.* (2009). XB130, a tissue-specific adaptor protein that couples the RET/PTC oncogenic kinase to PI 3-kinase pathway. *Oncogene* **28**: 937–949.

Matushansky I, Hernando E, Socci ND, Mills JE, Matos TA, Edgar MA *et al.* (2007). Derivation of sarcomas from mesenchymal stem cells via inactivation of the Wnt pathway. *J Clin Invest* **117**: 3248–3257.

Nagayama S, Fukukawa C, Katagiri T, Okamoto T, Aoyama T, Oyaizu N *et al.* (2005). Therapeutic potential of antibodies against FZD 10, a cell-surface protein, for synovial sarcomas. *Oncogene* **24**: 6201–6212.

Nagayama S, Katagiri T, Tsunoda T, Hosaka T, Nakashima Y, Araki N *et al.* (2002). Genome-wide analysis of gene expression in synovial sarcomas using a cDNA microarray. *Cancer Res* **62**: 5859–5866.

Nakayama R, Nemoto T, Takahashi H, Ohta T, Kawai A, Seki K *et al.* (2007). Gene expression analysis of soft tissue sarcomas: characterization and reclassification of malignant fibrous histiocytoma. *Mod Pathol* **20**: 749–759.

Nielsen TO, West RB, Linn SC, Alter O, Knowling MA, O'Connell JX *et al.* (2002). Molecular characterization of soft tissue tumours: a gene expression study. *Lancet* **359**: 1301–1307.

Ottaiano A, De Chiara A, Fazioli F, Talamanca AA, Mori S, Botti G *et al.* (2005). Biological prognostic factors in adult soft tissue sarcomas. *Anticancer Res* **25**: 4519–4526.

Overall CM, Kleifeld O. (2006). Tumour microenvironment—opinion: validating matrix metalloproteinases as drug targets and anti-targets for cancer therapy. *Nat Rev Cancer* **6**: 227–239.

Qian Y, Baisden JM, Westin EH, Guappone AC, Koay TC, Flynn DC. (1998). Src can regulate carboxy terminal interactions with AFAP-110, which influence self-association, cell localization and actin filament integrity. *Oncogene* **16**: 2185–2195.

Qian Y, Baisden JM, Zot HG, Van Winkle WB, Flynn DC. (2000). The carboxy terminus of AFAP-110 modulates direct interactions with actin filaments and regulates its ability to alter actin filament integrity and induce lamellipodia formation. *Exp Cell Res* **255**: 102–113.

Qian Y, Gatesman AS, Baisden JM, Zot HG, Cherezova L, Qazi I *et al.* (2004). Analysis of the role of the leucine zipper motif in regulating the ability of AFAP-110 to alter actin filament integrity. *J Cell Biochem* **91**: 602–620.

Shibata KR, Aoyama T, Shima Y, Fukiage K, Otsuka S, Furu M *et al.* (2007). Expression of the p16INK4A gene is associated closely with senescence of human mesenchymal stem cells and is potentially silenced by DNA methylation during *in vitro* expansion. *Stem Cells* **25**: 2371–2382.

Shima Y, Okamoto T, Aoyama T, Yasura K, Ishibe T, Nishijo K *et al.* (2007). *In vitro* transformation of mesenchymal stem cells by oncogenic H-rasVal12. *Biochem Biophys Res Commun* **353**: 60–66.

St-Pierre Y, Couillard J, Van Themsche C. (2004). Regulation of MMP-9 gene expression for the development of novel molecular targets against cancer and inflammatory diseases. *Expert Opin Ther Targets* **8**: 473–489.

Sun L, Hui AM, Su Q, Vortmeyer A, Kotliarov Y, Pastorino S *et al.* (2006). Neuronal and glioma-derived stem cell factor induces angiogenesis within the brain. *Cancer Cell* **9**: 287–300.

Toguchida J, Nakayama T. (2009). Molecular genetics of sarcomas: applications to diagnoses and therapy. *Cancer Sci* **100**: 1573–1580.

Toguchida J, Yamaguchi T, Ritchie B, Beauchamp RL, Dayton SH, Herrera GE *et al.* (1992). Mutation spectrum of the p53 gene in bone and soft tissue sarcomas. *Cancer Res* **52**: 6194–6199.

Wadayama B, Toguchida J, Shimizu T, Ishizaki K, Sasaki MS, Kotoura Y *et al.* (1994). Mutation spectrum of the retinoblastoma gene in osteosarcomas. *Cancer Res* **54**: 3042–3048.

Xu J, Bai XH, Lodyga M, Han B, Xiao H, Keshavjee S *et al.* (2007). XB130, a novel adaptor protein for signal transduction. *J Biol Chem* **282**: 16401–16412.

Zhang J, Park SI, Artime MC, Summy JM, Shah AN, Bomser JA *et al.* (2007). AFAP-110 is overexpressed in prostate cancer and contributes to tumorigenic growth by regulating focal contacts. *J Clin Invest* **117**: 2962–2973.

Supplementary Information accompanies the paper on the Oncogene website (http://www.nature.com/onc)

Spine

SPINE Volume 36, Number 11, pp E720–E726

DIAGNOSTICS

Impact of the O-C2 Angle on the Oropharyngeal Space in Normal Patients

Masato Ota, MD,* Masashi Neo, MD, PhD,* Tomoki Aoyama, MD, PhD,† Tatsuro Ishizaki, MD, PhD,‡ Shunsuke Fujibayashi, MD, PhD,* Mitsuru Takemoto, MD, PhD,* Takeo Nakayama, MD, PhD,‡ and Takashi Nakamura, MD, PhD,*

Study Design. Radiographic analysis using normal patients.

Objective. To analyze the relationship between the cervical alignment and the oropharyngeal space.

Summary of Background Data. Few clinical studies stress the effect of the occipito-C2 (O-C2) alignment on the oropharyngeal space. A previous study showed dysphagia and/or dyspnea after occipitocervical fusion was caused by oropharyngeal stenosis resulting from O-C2 fixation in a flexed position. Other independent researchers showed that development or improvement of obstructive sleep apnea in rheumatoid arthritis patients was related to the O-C2 alignment. However, there are limited basic data demonstrating the relationship between the O-C2 alignment and the oropharyngeal space.

Methods. Plain lateral cervical radiographs in five tested positions—neutral, flexion, extension, protrusion, and retraction—of 40 asymptomatic volunteers were collected. The O-C2 angle, the C2–C6 angle, and the anterior–posterior distance of the narrowest oropharyngeal airway space (nPAS) were measured, and the changes in value from the neutral to the other four positions were calculated for each patient.

Results. According to the multiple regression analysis, there was an extremely strong linear correlation of the change in the O-C2 angle with the percentage change in the nPAS. Referring to the multiple regression analysis, a decrease of 10° in the O-C2 angle caused a 37% reduction in the nPAS in the neutral position. In contrast, no significant correlation was found between the change in the C2–C6 angle and the percentage change in the nPAS.

Conclusion. Our results show the impact of the O-C2 angle on the oropharyngeal space. This knowledge will be useful for the diagnosis and treatment of the upper cervical lesion combined with the upper airway stenosis, and for the determination of the optimal fixation angle in occipitocervical fusion.

Key words: cervical alignment, protrusion, retraction, airway space, occipitocervical fusion, dysphagia, pharyngeal space.

Spine 2011;36:E720–E726

Dysphagia and/or dyspnea after posterior occipitocervical (O-C) fusion have been recognized as a serious postoperative complication.[1,2] The exact cause is unknown, but it is empirically known that a posterior total cervical fusion from the occiput to the thoracic spine in a flexed position may bring about these complications.[2,3] Therefore, many surgeons believe that the total sagittal alignment of the cervical spine is important to avoid these complications. However, optimal or safe cervical alignment is not known because it is complicated. It includes protrusion and retraction positions, and flexion and extension positions, and the reduction of atlantoaxial or vertical subluxation during operation also changes the alignment.[4–6] Therefore, it is widely believed to be safe that total O-C fusion should be performed after confirming the comfortable position using a halo-vest fixation.[2]

Recently, however, two quite different clinical studies have stressed the impact of the occipito-C2 (O-C2) alignment on the oropharyngeal space. The authors reported that the change in the alignment of a very short segment, that is, only O-C2, does impact the postoperative dysphagia and/or dyspnea by reducing the cross-sectional area of the oropharynx.[7] This conclusion was strongly supported by independent research by Ataka et al.[8] They revealed that obstructive sleep apnea (OSA) in rheumatoid arthritis (RA) patients with an upper cervical spine lesion improved after O-C fusion when the O-C2 was fixed in a more extended position. Conversely, OSA did not improve when their O-C2 alignment changed minimally after surgery. These two clinical researches from different standpoints suggest that the oropharyngeal space is not closely related with total cervical spine alignment but with O-C2 alignment. If this is true, it should impact the diagnosis and treatment of the upper cervical spine lesion.

From the *Department of Orthopaedic Surgery, Graduate School of Medicine, Kyoto University, Japan; †Department of Human Health Sciences, Graduate School of Medicine, Kyoto University, Japan; and ‡Department of Health Informatics, Kyoto University School of Public Health, Japan.

Acknowledgment date: April 29, 2010. First Revision date: August 24, 2010. Accepted date: August 27, 2010.

The paper submitted does not contain information about medical device(s)/drug(s).

No funds were received in support of this work. No benefits in any form have been or will be received from a commercial party related directly or indirectly to the subject of this paper.

IRB Approval: The Institutional Review Board of Kyoto University Hospital approved the protocol of this study.

Address correspondence and reprint requests to Masashi Neo, MD, PhD, Department of Orthopaedic Surgery, Graduate School of Medicine, Kyoto University, 54 Kawahara-cho, Shogoin, Sakyo-ku, Kyoto 606-8507, Japan; E-mail: neo@kuhp.kyoto-u.ac.jp

DOI: 10.1097/BRS.0b013e3181f9f714

A few basic studies have investigated the relationship between the pharyngeal space and head posture, but the changes in the partial range of motion between cervical flexion and extension were merely examined.[9–11] Neck posture in the sagittal plane not only includes flexion and extension, but also protrusion and retraction. Protrusion consists of upper cervical extension and lower cervical flexion, and *vice versa* for retraction.[4–6,12,13] Therefore, assessment of these two positions, and flexion and extension, is essential to evaluate the impact of the O-C2 alignment on the oropharyngeal space.

In this study, we investigated the correlation of the O-C2 angle with the oropharyngeal space based on data obtained using plain cervical lateral radiographs at different cervical positions in normal patients. The purpose of this study was to show the major impact of the O-C2 alignment on the oropharyngeal space.

MATERIALS AND METHODS

Patient Population

Forty healthy volunteers, 20 males and 20 females, participated in this study. None of the patients had a history of neck pain, cervical surgery, respiratory disease, or temporomandibular joint disorders. The mean age of the patients was 38.2 ± 10.5 years (range 22–57 years), and the mean body mass index (BMI) was 21.3 ± 2.7 kg/m^2 (range 16.8–27.0 kg/m^2).

Written informed consent was obtained from all patients after the potential risks, and the aim of the study and procedures for imaging, were fully explained. The Institutional Review Board of our institute approved the protocol of this study.

Setup and Data Collection

Five plain lateral radiographs of the cervical spine were taken for each patient while in a sitting posture on an upright chair. The initial radiograph was taken in the neutral position for reference, and the next four radiographs were taken in the flexion (chin-to-chest), extension (face toward ceiling), protrusion (maximal forward gliding of the head), and retraction (maximal backward gliding of the head) positions (Figure 1). In an attempt to minimize upper thoracic motion, patients were instructed to maintain both their upper thoracic spine and shoulders in close contact with the back of the chair throughout the tests. As shown in Figure 1A, the neutral position was determined by the correspondence between the facial shadow, connecting the most anterior point of glabela with the mental protuberance, and the gravity line drawn on the surface of the film board. In the protrusion and retraction positions (Figure 1D, E), care was taken to attain the same conditions as the neutral position mentioned above to hold the patient's head at zero sagittal rotation. Photographs were also taken under the following conditions. Patients were instructed to maintain their shoulders as low as possible to facilitate radiography of the C6 vertebral body and not to swallow just before the radiograph was taken. A radiograph was taken at the end of tidal expiration with the centric occlusal position. The radiographic film cassette was 200 cm from the radiograph tube. The imaging center was focused on the external acoustic meatus and all nasion, external occipital protuberance, and cervicothoracic junctions were included in the radiograph. One radiologic technologist, who had been strictly educated to set proper cervical positions under our guidance, took all the radiographs.

RADIOGRAPHIC MEASUREMENTS

On 200 lateral radiographs of the cervical spine, the O-C2 angle, the C2–C6 angle, and the narrowest oropharyngeal airway space (nPAS) were traced and measured to evaluate the relation between cervical alignment and the oropharyngeal airway space. The O-C2 angle was defined as the angle between the McGregor's line and the line parallel to the inferior endplate of C2, and the C2–C6 angle was defined as

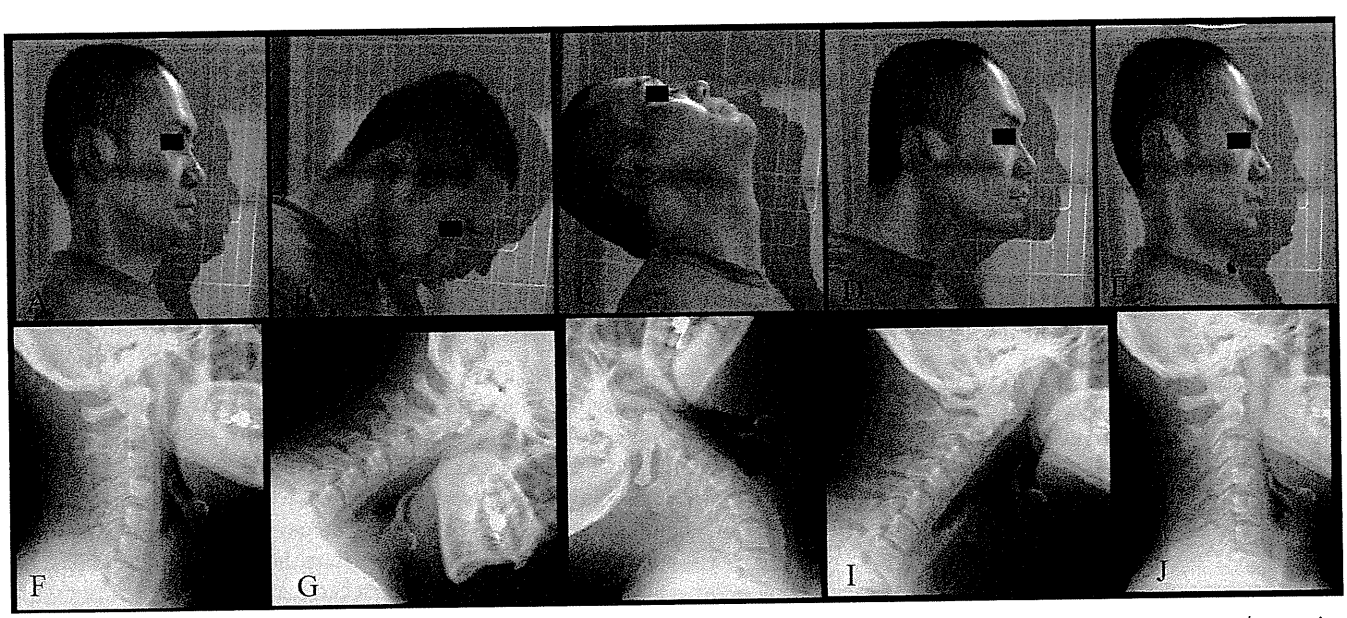

Figure 1. Five lateral cervical postures and radiographs in the neutral (**A**, **F**), flexion (**B**, **G**), extension (**C**, **H**), protrusion (**D**, **I**), and retraction (**E**, **J**) positions.

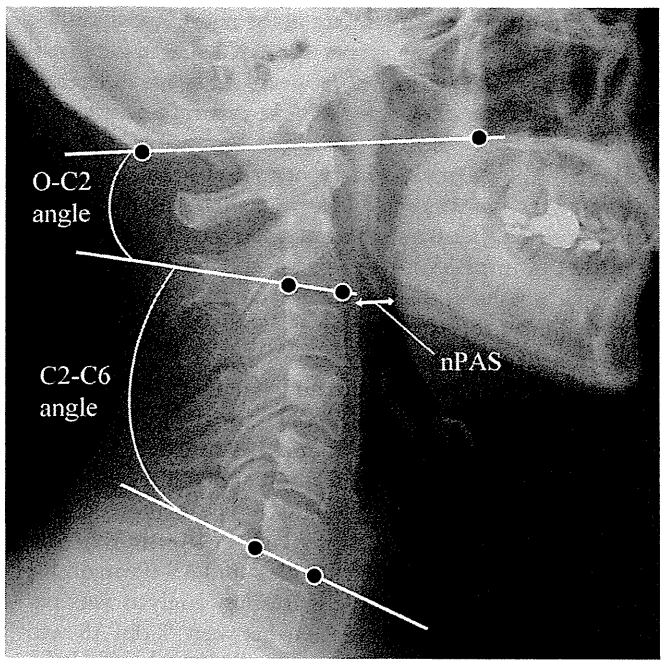

Figure 2. Representation of radiographic measurements. The O-C2 angle represents the angle between the McGregor's line and the inferior endplate of C2. The C2–C6 angle represents the angle between the inferior endplates of C2 and C6. nPAS represents the narrowest anterior–posterior distance from the posterior pharyngeal wall to the back of the tongue between the levels of the uvula tip and the epiglottis tip.

the angle between the lines parallel to the inferior endplate of C2 and C6 vertebral bodies (Figure 2). A positive value of both O-C2 and C2–C6 angles indicated a lordosis at the measured segments. The nPAS was obtained by measuring the shortest anterior–posterior distance from the posterior pharyngeal wall to the back of the tongue between the levels of the uvula tip and the epiglottis tip, as illustrated in Figure 2.

The first author traced and recorded all radiographic landmarks. To identify the landmarks accurately, the contrast and brightness of the images were regulated using a Centricity PACS system version 2.0 (GE healthcare, Milwaukee, WI). All linear and angular parameters were calculated with a precision of 0.1 mm and 0.1°, as dictated by this workstation. To ensure consistency, 100 randomly selected radiographs were traced and measured twice on another day. To evaluate the error of the method, the difference between the means of the first and second tracings for each of the variables was tested using paired *t* tests. No statistical significant difference was noted.

Evaluation of the Correlation of the O-C2 Angle or the C2–C6 Angle with the nPAS

To analyze the correlations of the O-C2 angle or the C2–C6 angle with the nPAS, the differences between the value in each of the four positions (X position), except the neutral position, and the value in the neutral position were calculated for each patient. The difference in the O-C2 angle (dOC2A) and C2–C6 angle (dC2C6A) were defined as dOC2A = O-C2 angle in X position – O-C2 angle in neutral position (degree) and dC2C6A = C2–C6 angle in X position – C2–C6 angle in neutral position (degree), respectively. To diminish the effect of the patient's body size on the pharyngeal space, the %dnPAS was employed as: %dnPAS = (nPAS in X position – nPAS in neutral position)/nPAS in neutral position × 100 (%).

STATISTICAL ANALYSIS

The means and standard deviations for the O-C2 angle, the C2–C6 angle, and the nPAS were calculated for each tested position. The values between the two positions were compared using the Tukey multiple comparison test. We used a multiple regression analysis to examine the association of %dnPAS with either dOC2A or dC2C6A, with %dnPAS as the dependent variable. The independent variables were age, sex, BMI, dOC2A, and dC2C6A. There were 160 analyzable data points from 40 patients, because each patient had a total of four data points to allow calculations for %dnPAS, dOC2A, and dC2C6A. In the regression model, we checked the assumptions of normality, linearity, homoscedasticity, and independence of the residuals. All reported *P* values are two-tailed, and the level of statistical significance was $P < 0.05$. We used SPSS software version 16.0 (SPSS Inc., Chicago, IL) for all analyses.

RESULTS

Table 1 lists the means and standard deviations for the O-C2 angle, the C2–C6 angle, and the nPAS for each tested

TABLE 1. Morphological Measurements

	Retraction (R) (n = 40)	Flexiontion (F) (n = 40)	Neutral (N) (n = 40)	Extension (E) (n = 40)	Protrusion (P) (n = 40)	Group difference* (P < 0.05)
O-C2 angle (°)	8.8 ± 6.5	11.6 ± 6.1	15.6 ± 6.7	35.1 ± 7.0	37.2 ± 8.4	E, P > N R < N
C2–C6 angle (°)	−6.3 ± 10.7	−24.7 ± 8.4	−2.1 ± 10.5	37.7 ± 9.8	1.1 ± 10.0	E > N F < N
nPAS (mm)	8.1 ± 3.5	10.6 ± 3.7	11.1 ± 3.2	18.4 ± 5.6	18.7 ± 5.4	E, P > N R < N

Note: Values are mean ± standard deviation.
**Tukey multiple comparison test.*
nPAS, the narrowest oropharyngeal airway space.

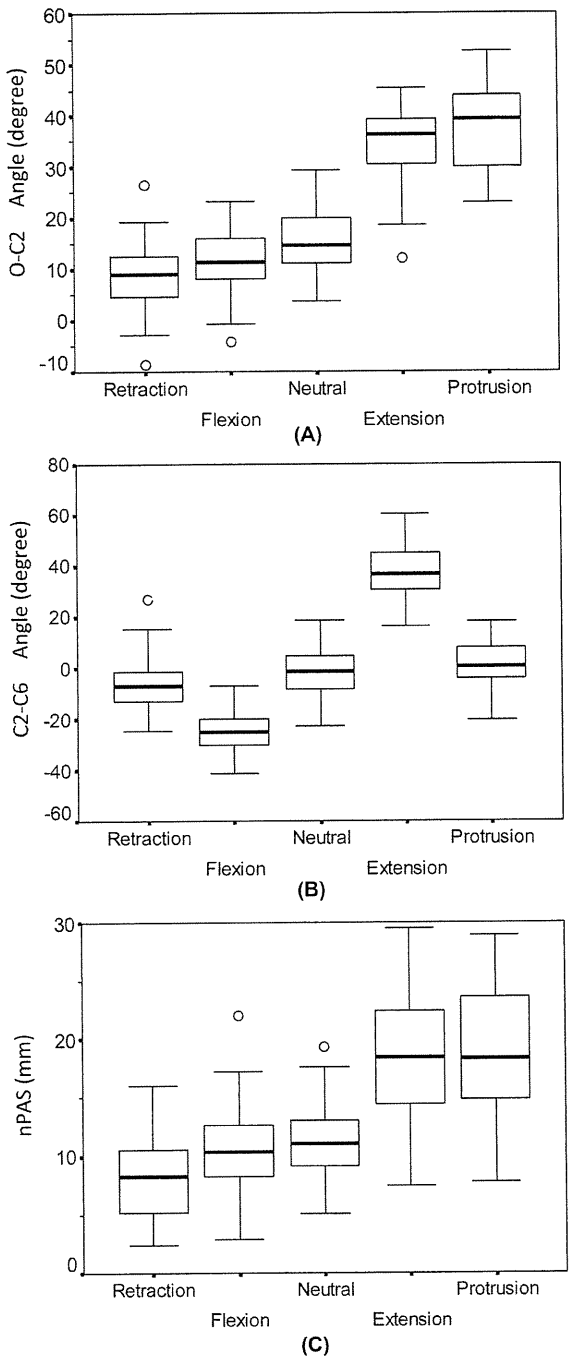

Figure 3. Box-and-whisker plots for each of the five tested positions. **A**, O-C2 angle; **B**, C2–C6 angle; **C**, nPAS. The patterns in A and C are the same but B is different. (nPAS represents the narrowest oropharyngeal airway space).

position. Figure 3 shows the box-and-whisker plots. The mean O-C2 angle in both extension and protrusion was significantly greater than that in the neutral position. The mean value in retraction was significantly smaller than in the neutral position, but no significant difference was found between the mean O-C2 angle in the flexion and neutral positions. The mean C2–C6 angle in extension was significantly greater than that in the neutral position, and the mean value in flexion was significantly smaller than that in the neutral position. On the other hand, the mean values of the C2–C6 angle in neither protrusion nor retraction showed significant differences compared with the C2–C6 angle in the neutral position. The mean nPAS in both extension and protrusion was significantly greater than the mean nPAS in the neutral position. The mean value in retraction was significantly smaller than that in the neutral position, but no significant difference was found between the mean nPAS in the flexion and neutral positions. Figure 3 clearly shows that the patterns of the box-and-whisker plots are almost the same for the O-C2 angle and the nPAS, but not for the C2–C6 angle.

Table 2 lists the mean values and standard deviations for dOC2A, dC2C6A, and %dnPAS. The scatter diagram between dOC2A and %dnPAS (Figure 4A) revealed that there was a strong positive linear correlation of dOC2A with %dnPAS (Pearson $r = 0.839$, $P < 0.001$). The scatter diagram between dC2C6A and %dnPAS (Figure 4B) showed that dC2C6A was weakly correlated with %dnPAS (Pearson $r = 0.392$, $P < 0.001$). A multiple regression analysis was performed to examine the association between %dnPAS with dOC2A, and dC2C6A (Table 3). The results identified that dOC2A was extremely correlated with %dnPAS [standardized regression coefficient (β) = 0.900, $P < 0.001$]. Conversely, no statistically significant correlation was found between dC2C6A and %dnPAS ($\beta = -0.082$, $P = 0.115$). The residual analyses revealed that the assumptions of normality, linearity, and homoscedasticity were not violated. Furthermore, 160 measurements obtained from 40 patients were analyzed using this multiple linear regression model and this might violate independence of the residuals in the model; however, the assumption of independence of the residuals was not violated (Durbin–Watson statistics = 1.96) in the model. The multiple regression equation was obtained as follows: %dnPAS = 3.71 × dOC2A − 0.20 × dC2C6A + 12.07 × WOMEN + 0.09 × AGE − 0.56 × BMI − 8.40 ($R^2 = 0.717$). This means that a decrease of 1° in dOC2A caused a reduction of 3.7% in the %dnPAS.

DISCUSSION

Oropharyngeal stenosis is speculated to be closely related to dysphagia and/or dyspnea after O-C fusion or OSA.[7,8,10,14,15] This study clearly shows that the occipito-upper-cervical alignment (O-C2 angle) has a great impact on the oropharyngeal space (nPAS), but that the middle-lower cervical alignment (C2–C6 angle) does not. It may be difficult to understand the significant relationship between the O-C2 angle and the nPAS intuitively because the occiput and C2 exist at a higher level than the oropharynx (Figure 2). This is probably the main reason why the close relationship between the O-C2 angle and the oropharyngeal stenosis has not been noticed by spinal surgeons thus far. Based on the previous reports,[7,8,14,16,17] we speculate that the mechanism of oropharyngeal stenosis caused by the reduction of the O-C2 angle is as follows. Soft tissue surrounds the oropharyngeal space, of which the anteriorly existing tongue root is the largest component. The soft tissue is then surrounded by a bony structure, the mandible

TABLE 2. Differences Between Each Position and the Neutral Position

	R–N	F–N	E–N	P–N
dOC2A (°)	−6.80 ± 3.53	−3.96 ± 4.57	19.5 ± 6.89	21.4 ± 8.90
dC2C6A (°)	−4.25 ± 7.76	−22.7 ± 7.91	39.8 ± 11.5	3.18 ± 10.5
%dnPAS (%)	−27.8 ± 20.2	−3.69 ± 26.0	68.2 ± 39.8	77.1 ± 58.0

Note: Values are mean ± standard deviation.

R, retraction; F, flexion; E, extension; P, protrusion; N, neutral; dOC2A = O-C2 angle in X position − O-C2 angle in neutral position; dC2C6A = C2–C6 angle in X position − C2–C6 angle in neutral position; %dnPAS = (nPAS in X position − nPAS in neutral position)/nPAS in neutral position × 100. (X position indicates flexion, extension, protrusion, or retraction position.)

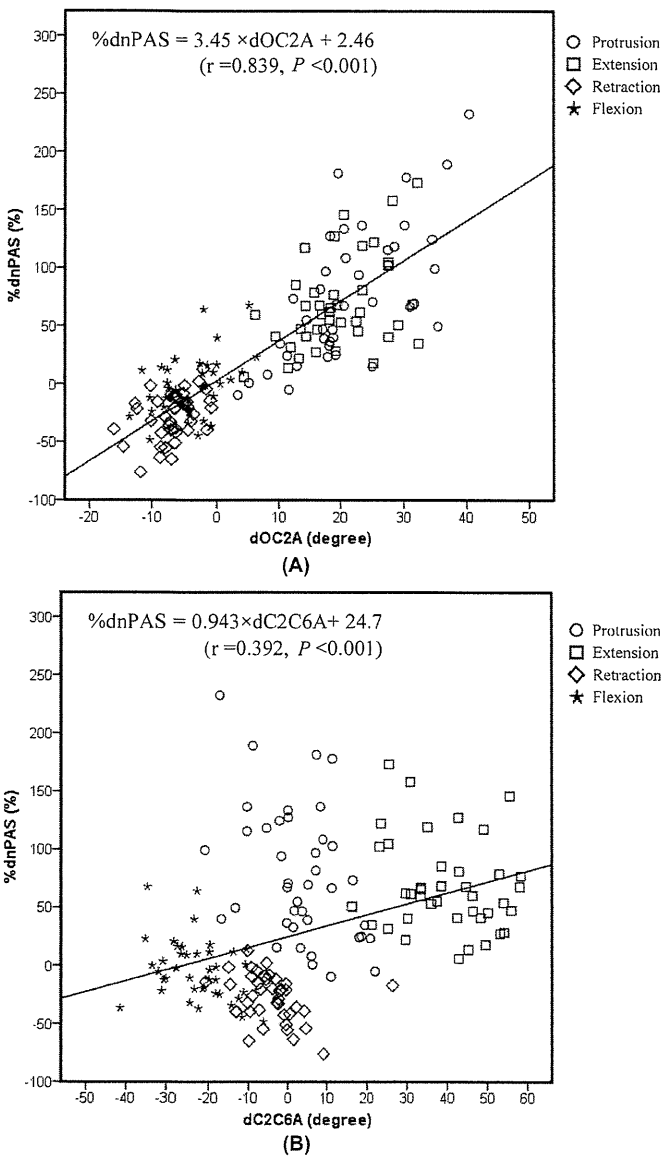

Figure 4. **A**, The scatter diagram between dOC2A and %dnPAS. **B**, The scatter diagram between dC2C6A and %dnPAS. dOC2A = O-C2 angle in X position − O-C2 angle in neutral position (degree); dC2C6A = C2–C6 angle in X position − C2–C6 angle in neutral position (degree); %dnPAS = (nPAS in X position − nPAS in neutral position)/nPAS in neutral position × 100 (%). (X position indicates flexion, extension, protrusion, or retraction position).

anteriorly and laterally, and the cervical spine posteriorly. The reduction of the O-C2 angle moves the maxilla in a flexed position, which makes the mandible shift posteriorly. This shift of the mandible reduces the volume of the bony container around the oropharyngeal level, resulting in an airway stenosis at this level. The authors previously found a downward displacement (posterior shift) of the tongue root in patients who developed a reduction in the O-C2 angle and subsequent dysphagia and/or dyspnea after O-C fusion.[7] This finding also supports the aforementioned mechanism.

Previous papers from different medical fields also support our conclusion. Muto et al, oral surgeons, investigated the relationship between the craniocervical inclination and the nPAS by measuring parameters at different degrees of cervical flexion and extension in the same patients.[10] They showed that the angle between the nasion-sella line (base line of the skull) and the tangent line of the posterior surface of C2 has close relationship to the nPAS. Their results are fairly consistent with this results, but our data are more convincing because we reached our conclusion by analyzing four different combinations of upper and lower cervical spine positions. Isono et al, anesthesiologists, endoscopically examined the cross-sectional area of the pharynx in completely anesthetized patients with OSA.[14] They clarified that protrusion was structurally beneficial to the maintenance of the pharyngeal airway because the change from the neutral to the protrusion position significantly enlarged it. Their results are also consistent with ours, because the O-C2 angle becomes larger in protrusion compared to the neutral position (Table 1 and Figure 3).

The O-C2 angle would be a very useful tool in spine surgery. It is well known that the major part of flexion and extension occurs at O-C1. We measured O-C2 angle, however, because it is much more popular to perform O-C2 fusion than O-C1 fusion, and O-C2 angle has been widely used as a landmark of O-C alignment.[1,7,8,18,19,20] In their previous study, the authors recommended that the O-C2 angle in O-C fusion should be kept at least at more than the preoperative O-C2 angle in the neutral position to prevent postoperative dysphagia and/or dyspnea.[7] Ataka et al showed that most of the OSA in RA patients with an upper cervical lesion is of an obstructive type because of a decreased O-C2 angle and subsequent oropharyngeal stenosis.[8] They also showed that O-C fusion with a more extended O-C2 position alleviates their symptoms. The measurement of the O-C2 alignment using the McGregor line and C2 endplate line has been proved to be

TABLE 3. Association of dOC2A or dC2C6A with %dnPAS from the Multiple Regression Analysis

		95% Confidence interval			
	B	Lower limit	Upper limit	β	*P*
dOC2A (°)	3.71	3.28	4.13	0.900	<0.001*
dC2C6A (°)	−0.197	−0.443	0.049	−0.082	0.115

All coefficients were adjusted for age, sex, and BMI.

R^2 = 0.717; B, unstandardized regression coefficient; β, standardized regression coefficient; dOC2A = O-C2 angle in X position − O-C2 angle in neutral position; dC2C6A = C2–C6 angle in X position − C2–C6 angle in neutral position; %dnPAS = (nPAS in X position − nPAS in neutral position)/nPAS in neutral position × 100. (X position indicates flexion, extension, protrusion, or retraction position.)

reproducible and is widely used.[7,8,18–20] The mean value of the O-C2 angle in the neutral position in this study was around 15°, which was consistent with previous reports.[18,19] However, its absolute value is variable between individuals,[19] and the change from the neutral position would be clinically more important. Therefore, we have no recommended O-C2 angle value. The greatest merit of the O-C2 angle is that it is easily measured using a C-arm during surgery. Usually it is difficult to determine the individual optimal cervical alignment macroscopically or radiographically in the prone position on the operating table. Although anatomic factors, such as obesity, micrognathia, and retrognathia, and dynamic factors, such as body positions and pharyngeal dilator muscle activities, also contribute to the development of dysphagia or OSA,[14,21–25] we believe that most of the deterioration after fusion surgery could be avoided by measuring the O-C2 angle and adjusting it before final fixation.

In this study, protrusion and retraction radiographs were used. Protrusion consists of upper cervical extension and lower cervical flexion, and *vice versa* for retraction. Ordway et al measured the motion of each vertebral segment in these positions,[4,5] and our results concerning the change of the O-C2 (upper cervical) and the C2–C6 (middle-lower cervical except C6/7) angles in each position are well consistent with their results. Spine surgeons should notice that these positions are quite different from flexion or extension when they perform O-C fusion. For example, it is risky for postoperative oropharyngeal stenosis to put a patient in the retraction position at O-C fusion to facilitate the access to the upper cervical region.

We also present quantitative data regarding the relationship between the O-C2 angle and the nPAS. The results from the multiple regression analysis indicate that a decrease in the O-C2 angle by 10° brings about a reduction of the oropharyngeal airway space in the neutral position of approximately 37%. Thus, a small change in O-C2 angle has a great impact on the oropharyngeal space, but it is very difficult to detect such a change macroscopically. This fact stresses the importance of the O-C2 angle measurement during surgery.

In conclusion, the authors showed that the O-C2 angle, among many factors, is a key to deciding the oropharyngeal space. This may be confirmed by further cadaver studies. The O-C2 angle is easily measured; therefore, it will be a simple and practical parameter in the diagnosis and treatment of the upper cervical lesion.

➢ Key Points

- ❑ Five lateral cervical radiographs taken in neutral, flexion, extension, protrusion, and retraction positions of 40 healthy volunteers were investigated as for cervical alignment and oropharyngeal space.
- ❑ The oropharyngeal space was not associated with C2–C6 alignment, but strongly correlated with O-C2 alignment.
- ❑ Based on the multiple regression analysis, a decrease in the O-C2 angle by 10° caused a reduction of the narrowest oropharyngeal airway space in the neutral position of approximately 37%.
- ❑ The O-C2 angle would be a simple and practical parameter in the diagnosis and treatment of the upper cervical lesion with the oropharyngeal stenosis, and for the determination of the optimal fixation angle in occipitocervical fusion.

Acknowledgments

The authors thank the following individuals for their helpful discussion in this study: Prof. Kazuo Chin, Department of Respiratory Care and Sleep Control Medicine, Graduate School of Medicine, Kyoto University, Kyoto, Japan; and Dr. Tomohiro Handa and Dr. Kensaku Aihara, Department of Respiratory Medicine, Graduate School of Medicine, Kyoto University, Kyoto, Japan. The authors are also grateful to the radiologic technologists who cooperated in taking radiographs, Mr. Ryuzou Tanaka, Mr. Kenichi Ogawa, Mrs. Sakiko Himeji, and Mr. Kohei Yamaoka.

References

1. Yoshida M, Neo M, Fujibayashi S, et al. Upper-airway obstruction after short posterior occipitocervical fusion in a flexed position. *Spine* 2007;32:E267–70.
2. Bagley CA, Witham TF, Pindrik JA, et al. Assuring optimal physiologic craniocervical alignment and avoidance of swallowing-related complications after occipitocervical fusion by preoperative halo vest placement. *J Spinal Disord Tech* 2009;22:170–76.
3. Matsuyama Y, Kawakami N, Yoshihara H, et al. Long-term results of occipitothoracic fusion surgery in RA patients with destruction of the cervical spine. *J Spinal Disord Tech* 2005;18(Supp 1):S101–6.
4. Ordway NR, Seymour R, Donelson RG, et al. Cervical sagittal range-of-motion analysis using three methods: Cervical range-of-motion device, 3space, and radiography. *Spine* 1997;22:501–8.

5. Ordway NR, Seymour RJ, Donelson RG, et al. Cervical flexion, extension, protrusion, and retraction: a radiographic segmental analysis. *Spine* 1999;24:240–7.
6. Maeda T, Saito T, Harimaya K, et al. Atlantoaxial instability in neck retraction and protrusion positions in patients with rheumatoid arthritis. *Spine* 2004;29:757–62.
7. Miyata M, Neo M, Fujibayashi S, et al. O-C2 angle as a predictor of dyspnea and/or dysphagia after occipitocervical fusion. *Spine* 2009;34:184–8.
8. Ataka H, Tanno T, Miyashita T, et al. Occipitocervical fusion has potential to improve sleep apnea in patients with rheumatoid arthritis and upper cervical lesions. *Spine* 2010;35:E971–5.
9. Hellsing E. Changes in the pharyngeal airway in relation to extension of the head. *Eur J Orthodontics* 1989;11:359–65.
10. Muto T, Takeda S, Kanazawa M, et al. The effect of head posture on the pharyngeal airway space (PAS). *Int J Oral Maxillofac Surg* 2002;31:579–83.
11. Anegawa E, Tsuyama H, Kusukawa J, et al. Lateral cephalometric analysis of the pharyngeal airway space affected by head posture. *Int J Oral Maxillofac Surg* 2008;37:805–9.
12. Penning L. Normal movements of the cervical spine. *AJR Am J Roentgenol* 1978;130:317–26.
13. Penning L. Acceleration injury of the cervical spine by hypertranslation of the head: Part I. Effect of normal translation of the head on cervical spine motion: a radiological study. *Eur Spine J* 1992;1:7–12.
14. Isono S, Tanaka A, Ishikawa T, et al. Sniffing position improves pharyngeal airway patency in anesthetized patients with obstructive sleep apnea. *Anesthesiology* 2005;103:489–94.
15. Verbraecken JA, Backer WA. Upper airway mechanics. *Respiration* 2009;78:121–33.
16. Kuna ST, Remmers JE. Anatomy and physiology of upper airway obstruction. In:Kryger MH, Roth T, Dement WC eds. *Principles and Practice of Sleep Medicine*. 3 ed. Philadelphia: WB Saunders, 2000:840–58.
17. Inoko Y, Morita O. Influence of oral appliances on craniocervical posture in obstructive sleep apnea-hypopnea syndrome patients. *J Prosthodontic Res* 2009;53:107–10.
18. Matsunaga S, Onishi T, Sakou T. Significance of occipitoaxial angle in subaxial lesion after occipitocervical fusion. *Spine* 2001;26:161–5.
19. Shoda N, Takeshita K, Seichi A, et al. Measurement of occipitocervical angle. *Spine* 2004;29:E204–8.
20. Logroscino CA, Genitiempo M. Relevance of the cranioaxial angle in the occipitocervical stabilization using an original construct: a retrospective study on 50 patients. *Eur Spine J* 2009;18(Supp 1):S7–12.
21. Isono S, Tanaka A, Tagaito Y, et al. Influences of head positions and bite opening on collapsibility of the passive pharynx. *J Appl Physiol* 2004;97:339–46.
22. Tsuiki S, Almeida FR, Bhalla PS, et al. Supine-dependent changes in upper airway size in awake obstructive sleep apnea patients. *Sleep Breathing* 2003;7:43–50.
23. Ono T, Otsuka R, Kuroda T, et al. Effects of head and body position on two- and three-dimensional configurations of the upper airway. *J Dent Res* 2000;79:1879–84.
24. Zhang W, Masumi S, Makihara E, et al. Effects of jaw, head and body positions on upper airway dimensions and maximum forced inspiratory airflow. *J Kyushu Dent Soc* 2009;63:8–17.
25. Soga T, Nakata S, Yasuma F, et al. Upper airway morphology in patients with obstructive sleep apnea syndrome: effects of lateral positioning. *Auris Nasus Larynx* 2009;36:305–9.